© 2014. Published by The Company of Biologists Ltd | Journal of Cell Science (2014) 127, 1684–1698 doi:10.1242/jcs.133892

RESEARCH ARTICLE

Regulation of Src trafficking and activation by the endocytic regulatory proteins MICAL-L1 and EHD1

James B. Reinecke, Dawn Katafiasz, Naava Naslavsky and Steve Caplan*

ABSTRACT

Localization of the non-receptor tyrosine kinase Src to the cell periphery is required for its activation and to mediate focal adhesion turnover, cell spreading and migration. Inactive Src localizes to a perinuclear compartment and the movement of Src to the plasma membrane is mediated by endocytic transport. However, the precise pathways and regulatory proteins that are responsible for SRC transport are incompletely understood. Here, we demonstrate that Src partially colocalizes with the endocytic regulatory protein MICAL-L1 (molecule interacting with CasL-like protein 1) in mammalian cells. Furthermore, MICAL-L1 is required for growth-factor- and integrin-induced Src activation and transport to the cell periphery in HeLa cells and human fibroblasts. Accordingly, MICAL-L1 depletion impairs focal adhesion turnover, cell spreading and cell migration. Interestingly, we find that the MICAL-L1 interaction partner EHD1 (EH domain-containing protein 1) is also required for Src activation and transport. Moreover, the MICAL-L1-mediated recruitment of EHD1 to Src-containing recycling endosomes is required for the release of Src from the perinuclear endocytic recycling compartment in response to growth factor stimulation. Our study sheds new light on the mechanism by which Src is transported to the plasma membrane and activated, and provides a new function for MICAL-L1 and EHD1 in the regulation of intracellular non-receptor tyrosine kinases.

KEY WORDS: Endocytic recycling, Focal adhesion, MICAL-L1, EHD1, Migration, Src, Circular dorsal ruffle

INTRODUCTION

Cell adhesion and migration are fundamental processes that contribute to normal physiological functions such as organ development, tissue maintenance and homeostasis. These processes are also intricately involved in pathological conditions such as wound healing, atherosclerosis and cancer (Friedl and Gilmour, 2009). The non-receptor tyrosine kinase Src, the founding member of the Src family kinases (SFKs), plays key roles in regulating cell adhesion and migration (Fincham and Frame, 1998), and the deregulation of Src kinase activity in cancer is correlated with metastasis and poor survival (Wheeler et al., 2009). Each SFK is characterized by a prototypical structure defined by: an N-terminal SH4 lipid-modification domain (Koegl et al., 1994), an unique domain, a type-II proline-rich-binding SH3 domain, a phospho-tyrosine-binding SH2 domain (Payne et al., 1993), a proline-rich linker region, an SH1 kinase domain containing a crucial autophosphorylation site (Smart et al., 1981), and a C-terminal regulatory domain (Cooper et al., 1986) containing a crucial tyrosine residue (Y529 in human Src) that is phosphorylated by C-terminal Src kinase (CSK) (Nada et al., 1991).

The domain architecture of Src is central to regulating its kinase activity (Xu et al., 1999). The phosphorylation of Y529 promotes an intramolecular interaction with its SH2 domain, which in turn brings the proline-rich SH2-kinase linker domain into close proximity with the SH3 domain, thus preventing Src kinase activity. The activation of receptor tyrosine kinases such as the epidermal growth factor receptor (EGFR) and the platelet-derived growth factor receptor (PDGFR) (Kypta et al., 1990; Luttrell et al., 1994; Mori et al., 1993), or the engagement of integrin receptors with the extracellular matrix (Arias-Salgado et al., 2003), promotes protein–protein interactions with the SH3 or SH2 domain, or dephosphorylation of Y529 (Ren et al., 2004). This in turn alleviates the Src intramolecular interaction and facilitates kinase activity. Once activated, Src phosphorylates multiple proteins that promote changes in membrane dynamics through the modulation of Rho GTPase activity (Timpson et al., 2001), focal adhesion disassembly (Fincham and Frame, 1998) and rearrangement of the actin cytoskeleton (Chang et al., 1995; Tanji et al., 2010), all of which collectively contribute to cell migration.

Although the biochemical regulation of Src is one mechanism by which its kinase activity is regulated, it is now apparent that the modulation of the intracellular localization of Src is an important regulatory mechanism (Sandilands and Frame, 2008). Initial studies demonstrated that v-Src (constitutively active Src that is the oncogenic component of the Rous sarcoma virus) localizes to the plasma membrane and cytoplasmic compartments (Courtneidge et al., 1980; Rohrschneider, 1979). Subsequently, the use of temperature-sensitive mutants of v-Src that are inactive at 41℃ and active at 35℃ demonstrated that inactive v-Src localizes to the perinuclear region and, upon activation, translocates to peripheral membranes and focal adhesions (Welham and Wyke, 1988) to promote focal adhesion turnover and cell migration (Fincham and Frame, 1998).

Similarly, inactive Src localizes to perinuclear endosomes, whereas active Src localizes to focal adhesions (Kaplan et al., 1994; Kaplan et al., 1992). Elegant work by Sandilands et al. (Sandilands et al., 2004) using wild-type Src expressed in Src-null mouse embryonic fibroblasts provided clear evidence that Src translocates to the cell periphery in an actin-dependent manner within endocytic vesicles containing the small GTPase RhoB. Disruption of the actin cytoskeleton by cytochalasin D or by genetic ablation of RhoB prevented Src translocation and activation (Sandilands et al., 2004). Data from other groups

Department of Biochemistry and Molecular Biology and Eppley Cancer Center, University of Nebraska Medical Center, Omaha, NE 68198, USA.

*Author for correspondence (scaplan@unmc.edu)

Received 25 April 2013; Accepted 6 January 2014

Journal of Cell Science

Journal of Cell Science (2014) 127, 1684–1698 doi:10.1242/jcs.133892

suggest that the trafficking of Src occurs through late endosomes (Kasahara et al., 2007), regulated by the endosomal sorting complexes required for transport (ESCRT) machinery (Tu et al., 2010). However, the effect of ESCRT depletion on Src activity might be indirect, as the ESCRT complex regulates the trafficking and localization of integrins in human fibroblasts (Lobert and Stenmark, 2012). Regardless, the endocytic regulatory proteins that are involved in Src localization remain largely uncharacterized.

Work from our laboratory and others has shown that Eps15 homology (EH) domain-containing protein 1 (EHD1) and its interacting partner MICAL-L1 (molecule interacting with CasL-like protein 1) are required for the exit of transmembrane receptors from the perinuclear endocytic recycling compartment (ERC) (Caplan et al., 2002; Sharma et al., 2009). Although MICAL-L1 and EHD1 are crucial mediators of receptor recycling to the plasma membrane, the potential role of MICAL-L1 and EHD1 in regulating the intracellular trafficking and function of non-receptor tyrosine kinases, such as Src, has not been established. We hypothesized that MICAL-L1 and EHD1 might be required for Src transport to the cell periphery and thus might be regulators of Src-dependent functions. We demonstrate herein that Src localizes to MICAL-L1-positive endocytic compartments. Furthermore, the depletion of either MICAL-L1 or EHD1 impairs Src activation and its localization to the cell periphery following treatment with growth factor. Functionally, we show that the loss of MICAL-L1 impairs focal adhesion turnover, cell spreading and cell migration. We now demonstrate that inactive Src is concentrated in the perinuclear ERC and that, upon growth factor treatment, EHD1 is recruited to MICAL-L1-positive structures and promotes the release of Src from the ERC, allowing Src to travel to the plasma membrane an thereby affecting key downstream cellular processes.

RESULTS

MICAL-L1 associates with Src in mammalian cells and is required for Src activation and localization to the cell periphery

In HeLa cells, MICAL-L1 displays a unique localization, decorating long tubular endosomes that emanate from the ERC [(Sharma et al., 2009) and Fig. 1B]. Under steady-state conditions, we observed that endogenous Src partially colocalized with MICAL-L1 along tubular membranes that radiate from the ERC (Fig. 1A,B, arrows in inset). Given that Src family members, such as Fyn and Yes, might also be expressed in HeLa cells, we next overexpressed Src–GFP and HA–MICAL-L1 fusion proteins in Src, Yes and Fyn (SYF)-null mouse embryonic fibroblasts to test whether MICAL-L1 specifically associates with Src in mammalian cells. Under steady-state conditions, Src–GFP was concentrated along membrane ruffles and tubulo-vesicular structures underneath the plasma membrane (Fig. 1D, arrows). HA–MICAL-L1 was also found to associate with these structures (Fig. 1E, arrows), and it partially colocalizes with Src–GFP (Fig. 1F, merge), suggesting that MICAL-L1 specifically associates with Src and not other Src family members such as Yes and Fyn. Although Src and MICAL-L1 could consistently be observed in an immunoprecipitation complex with low intensity (data not shown), it is likely that the insolubility of membrane-associated Src renders this interaction minimal (Fra et al., 1994). Moreover, the failure to detect an interaction by using yeast two-hybrid experiments (data not shown) suggests that the interaction is indirect. These data support the hypothesis that there is transient MICAL-L1–Src interaction, consistent with the interactions described between Src and other proteins involved in regulating its transport (Sandilands et al., 2004; Tu et al., 2010).

Given that Src localizes to MICAL-L1-decorated endosomal structures, we hypothesized that MICAL-L1 regulates the

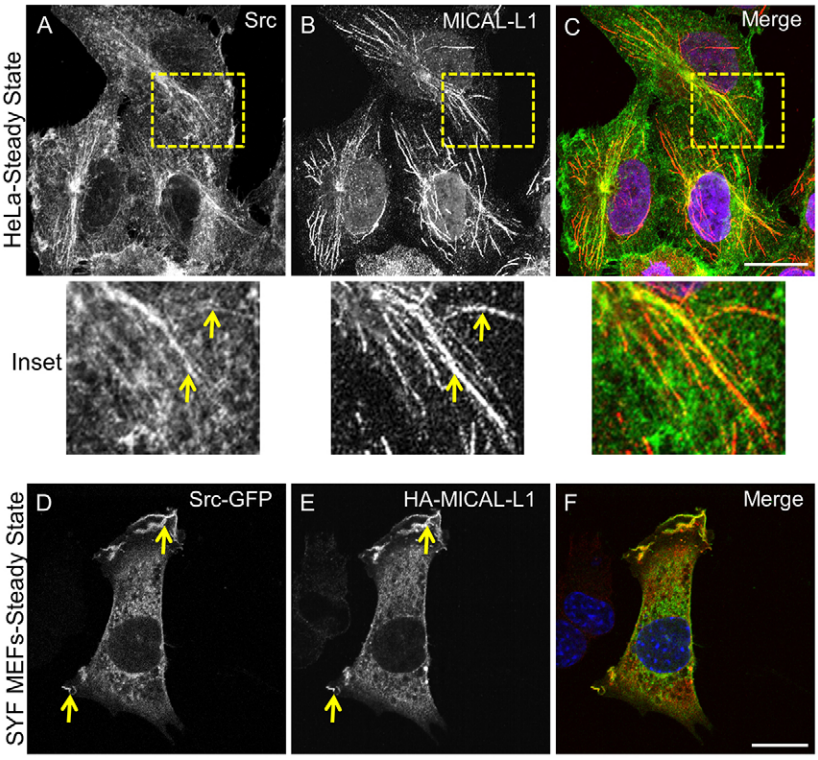

Fig. 1. Partial colocalization between MICAL-L1 and Src in mammalian cells. (A–C) Immunofluorescence demonstrating partial colocalization of endogenous Src (A) along endogenous MICAL-L1-decorated tubular endosomes (B) in HeLa cells as marked by arrows in inset. (D–F) Overexpressed Src–GFP (D) partially colocalizes with HA–MICAL-L1 (E) in SYF fibroblasts (arrows). Blue, DNA stained with DAPI. Scale bars: 10 μm.

Journal of Cell Science (2014) 127, 1684–1698 doi:10.1242/jcs.133892

activation and transport of Src. Src autophosphorylation on tyrosine (Y)419 (in humans) is required for its kinase activity (Feder and Bishop, 1990; Reuter et al., 1990) and serves as a marker for Src activation. In HeLa cells that were treated with control small interfering (si)RNA, stimulation with epidermal growth factor (EGF) caused a time-dependent increase in Src activation (Fig. 2A, lanes 1–3). However, in cells treated with siRNA specific to MICAL-L1, >95% of the MICAL-L1 was depleted, and the levels of Src Y419 phosphorylation (Src-pY419) failed to increase above the baseline observed in serum-starved cells (Fig. 2A, lanes 4–6). This indicates that MICAL-L1 is required for EGF-induced Src activation. In agreement with these findings, MICAL-L1 depletion inhibited the localization of active Src (green) to paxillin-positive peripheral focal adhesions (red) (compare Fig. 2B to 2C, see line-scan analysis).

We hypothesized that MICAL-L1 knockdown (KD) directly impacts upon Src localization and activation. It was therefore necessary to rule out the possibility that MICAL-L1 might indirectly impair EGF-induced Src activation by affecting the levels of EGFR at the cell surface, or EGFR endocytosis. By using flow cytometry with fluorescently labeled EGF, we found that MICAL-L1-depleted cells displayed a small increase in EGF-binding capacity compared to control cells (supplementary material Fig. S1A,B), indicating that a lack of EGFR on the plasma membrane is not the underlying cause of reduced Src

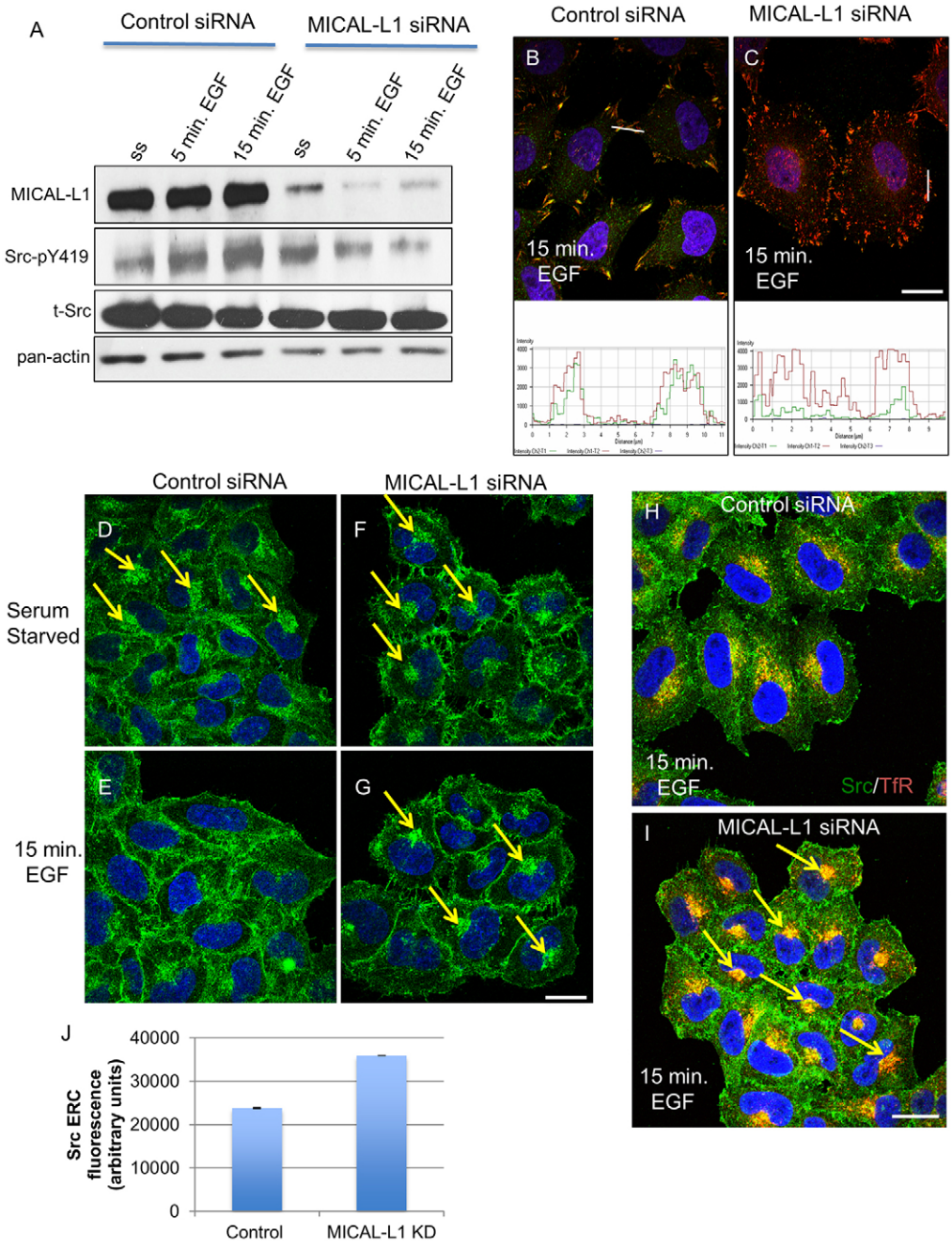

Fig. 2. MICAL-L1 depletion in HeLa cells impairs EGF-induced Src activation and translocation out of the ERC. (A) An immunoblot of control (lanes 1–3) and MICAL-L1-depleted HeLa cells (lanes 4–6) demonstrating reduced EGF-induced Src activation as measured by Src autophosphorylation (Src-pY419) upon MICAL-L1 depletion. SS, serum starved. (B,C) Control (B) and MICAL-L1-KD (C) cells were stimulated with EGF for 15 min, fixed and labeled with antibodies against Src-pY419 (green) and paxillin (red). Profile analysis of two individual focal adhesions demonstrates the recruitment of active Src to paxillin-containing focal adhesions in control (B) but not MICAL-L1-KD cells (C). (D–G) Under serum-starved (SS) conditions, total Src (green) localizes to the perinuclear region (arrows) in control (D) and MICAL-L1-siRNA-treated cells (F). In response to EGF, Src translocates from the ERC to the plasma membrane in control cells (E) but is largely retained in the ERC in MICAL-L1-KD cells (G, arrows). (H–J) Cells were stimulated with EGF, and stained for Src (green) and transferrin receptor (TfR, red). Note the increased overlap of Src and TfR at the ERC in MICAL-L1-KD cells (I, yellow arrows) compared to control (H). (J) ImageJ was used to quantify Src fluorescence in the TfR-positive ERC after EGF stimulation, and one-way ANOVA showed that there was significantly more Src in MICAL-L1 KD compared to control ($P<0.01$). Error bars show s.e.m. Blue, DNA stained with DAPI. Scale bars: 10 μm.

Journal of Cell Science

Journal of Cell Science (2014) 127, 1684–1698 doi:10.1242/jcs.133892

activation upon MICAL-L1 KD. To evaluate whether MICAL-L1 KD affects EGFR internalization, cells were pulsed with unlabeled EGF for 15 min and were immunostained with antibodies against EGFR. MICAL-L1-KD cells displayed no overt defects in EGFR trafficking (supplementary material Fig. S1C–F). Finally, MICAL-L1 depletion did not affect EGFR phosphorylation upon stimulation with EGF (supplementary material Fig. S1G, compare levels of EGFR-pY1068). Of note, Src does regulate EGFR trafficking (Donepudi and Resh, 2008; Ware et al., 1997; Wilde et al., 1999). Thus, MICAL-L1 KD might have subtle effects on Src-dependent EGFR trafficking. Given that MICAL-L1 KD has minimal effects on EGF binding and EGFR activation, we concluded that the decreased Src activation in MICAL-L1-KD cells is not due to indirect effects.

The failure of active Src to localize to the cell periphery upon MICAL-L1 depletion raised the question of its subcellular distribution under these conditions. To address this, we used an antibody that recognized both the phosphorylated and non-phosphorylated forms of Src, and monitored Src localization by immunofluorescence microscopy in the presence or absence of MICAL-L1. In serum-starved cells either in the presence (Fig. 2D) or absence (Fig. 2F) of MICAL-L1, Src was observed throughout the cell (including at the plasma membrane) but displayed a concentrated presence in the perinuclear region (arrows). In cells treated with control siRNA, stimulation with EGF caused Src to disperse from the perinuclear region and to display enhanced localization underneath the plasma membrane (Fig. 2E). However, in MICAL-L1-depleted cells, the majority of Src remained in the perinuclear region upon EGF stimulation (Fig. 2G, arrows), indicating that MICAL-L1 is required for Src transport from this region to the plasma membrane.

Given that there are contradictory reports as to whether inactive Src localizes to the ERC (Sandilands et al., 2004) or to late endosomes (Kasahara et al., 2007; Tu et al., 2010), we addressed the nature of the perinuclear region in which Src is retained upon MICAL-L1 depletion. We stimulated cells with EGF and immunostained for Src and for the transferrin receptor (TfR), a well-established marker of the ERC that is absent in late endosomes. Compared to EGF-stimulated control cells, which display modest overlap between Src and TfR (Fig. 2H), MICAL-L1 depletion resulted in substantial accumulation and overlap of Src and TfR in the ERC (Fig. 2I, yellow arrows). Quantification of Src fluorescence in the TfR-positive ERCs indicated that it was significantly higher in MICAL-L1-KD cells (Fig. 2J). Accordingly, MICAL-L1 colocalizes with endogenous Src in HeLa cells (Fig. 1) and regulates EGF-induced Src activation by controlling the exit of Src from the ERC (Fig. 2).

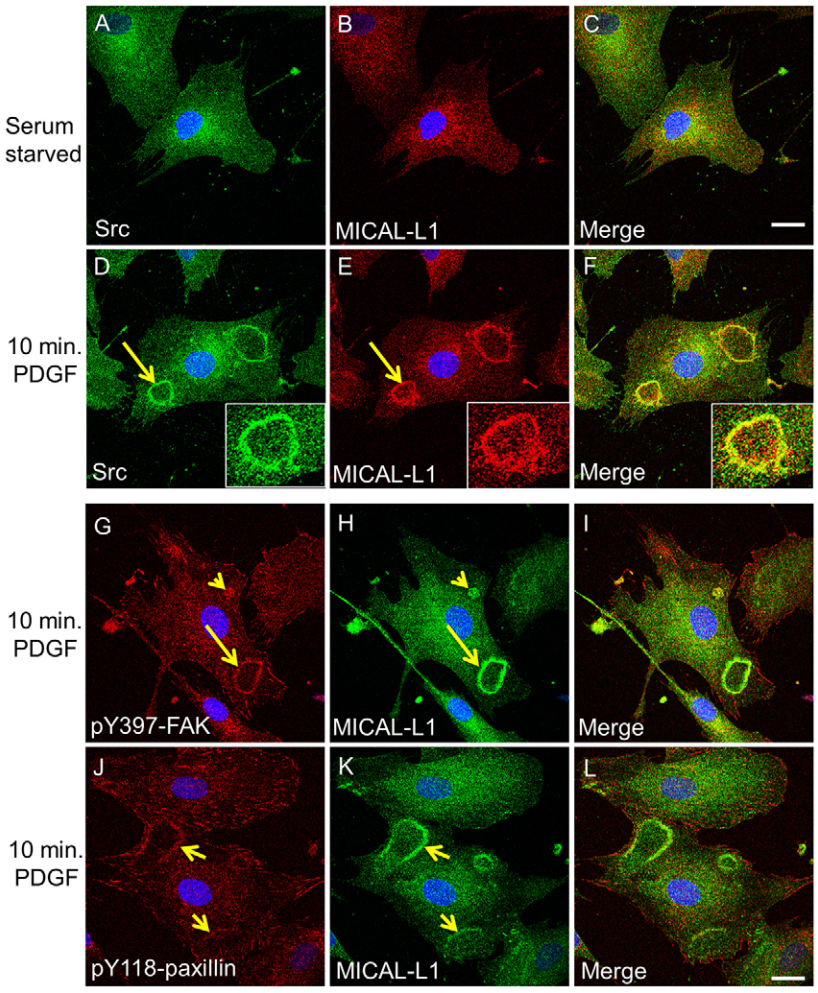

Fig. 3. MICAL-L1 colocalizes with Src and focal adhesion proteins along CDRs in human foreskin fibroblasts (BJ). (A–F) BJ cells were serum starved (A–C) or stimulated with 15 ng/ml PDGF (D–F) for 10 min. Immunofluorescence of Src (green) and MICAL-L1 (red) demonstrates their colocalization along CDRs (arrows, see inset). (G–L) BJ cells were stimulated with PDGF and stained for MICAL-L1 (green) and FAK-pY397 (red, G) or paxillin-pY118 (red, J). Arrows depict colocalization along CDRs. Arrowheads mark colocalization of MICAL-L1 and FAK-pY397 on macropinocytic-like vesicles. Blue, DNA stained with DAPI. Scale bars: 10 μm.

Journal of Cell Science (2014) 127, 1684–1698 doi:10.1242/jcs.133892

MICAL-L1 colocalizes with Src and is required for its recruitment to circular dorsal ruffles in human foreskin fibroblasts following PDGF stimulation

Although we found that MICAL-L1 partially colocalized with Src and regulated its endocytic trafficking in HeLa cells upon EGF stimulation (Figs 1, 2), it was unclear whether MICAL-L1 colocalized with Src in other cells such as normal human fibroblasts and whether the regulation of Src by MICAL-L1 is specific to EGF or constitutes part of a more general regulatory mechanism. In Src-null mouse embryonic fibroblasts, transfected Src translocates from the ERC to the plasma membrane ruffles upon stimulation with platelet-derived growth factor (PDGF) (Sandilands et al., 2004). However, the localization of endogenous Src in human fibroblasts following PDGF stimulation has not been characterized. In human foreskin fibroblasts (BJ cells), Src localized to circular dorsal ruffles (CDRs) following PDGF stimulation (CDR; compare Fig. 3A to 3D, see arrow). Similarly, PDGF stimulation resulted in MICAL-L1 recruitment to CDRs, where it colocalized with Src (Fig. 3D–F, arrow, and see insets), suggesting that the colocalization of MICAL-L1 and Src is physiologically relevant in normal human cells. MICAL-L1 also colocalized with other focal adhesion regulatory proteins such as phosphorylated tyrosine 397 of focal adhesion kinase (FAK, also known as PTK2) (Fig. 3G–I, pY397-FAK, arrow and arrowhead) and phosphorylated tyrosine 118 of paxillin (Fig. 3J–L, pY118-paxillin, arrows).

Given that MICAL-L1 and Src colocalize along CDRs and that Src activity is required for CDR formation and macropinocytosis (Mettlen et al., 2006; Veracini et al., 2006), we tested whether MICAL-L1 is required for Src localization to CDRs in BJ cells. Control and MICAL-L1-depleted BJ cells were stimulated with

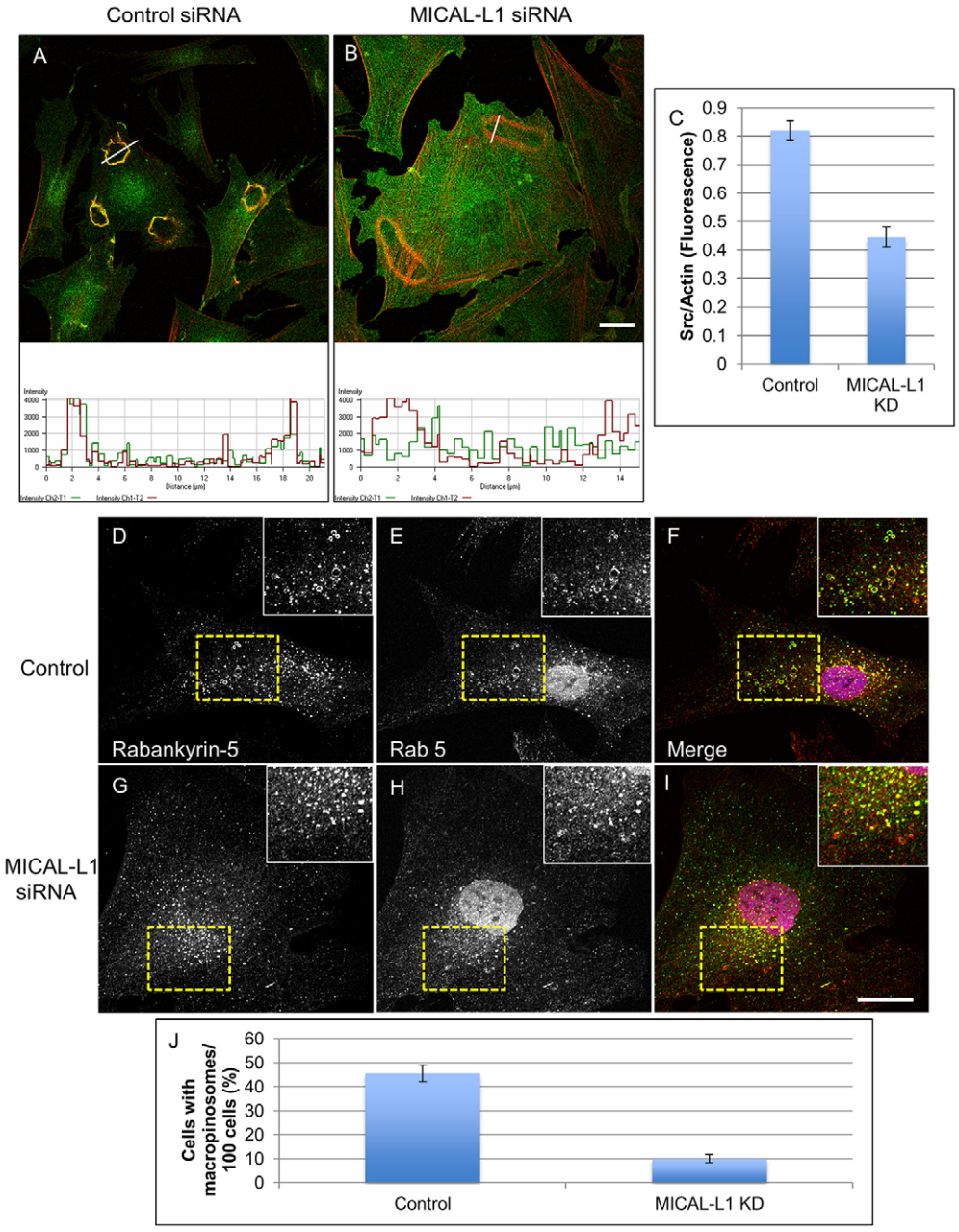

Fig. 4. MICAL-L1 regulates Src recruitment to CDRs. (A–C) Control (A) and MICAL-L1-KD cells (B) were stimulated with PDGF for 10 min, fixed and stained with Src (green) and phalloidin to show F-actin (red). Src recruitment to CDRs was then quantified using profile analysis (C). (D–J) Control (D–F) and MICAL-L1-KD cells (G–I) were stimulated with PDGF for 20 min and stained with antibodies against Rabankyrin-5 (green) and Rab5 (red) to mark macropinosomes (yellow arrows). Cells containing macropinosomes were manually counted in 100 cells per experiment (J). Error bars show s.e.m. Blue, DNA stained with DAPI. Scale bars: 10 μm.

Journal of Cell Science (2014) 127, 1684–1698 doi:10.1242/jcs.133892

PDGF for 10 min and were stained with Src and phalloidin (to mark actin). In control cells, Src localized to uniformly round actin-rich CDRs (Fig. 4A). By contrast, MICAL-L1 KD resulted in a significant reduction in the recruitment of Src to CDRs (Fig. 4B, quantified in 4C), and the structures were frequently elliptical rather than circular (Fig. 4B). In addition, the size of MICAL-L1-KD cells was typically greater than that of control cells (compare Fig. 4B to 4A; compare Fig. 5D–F to 5A–C, and see cell-spreading experiments in Fig. 7A–D). To assess whether MICAL-L1 KD affected the maturation of CDRs into macropinocytic vesicles, we quantified the number of cells that contained enlarged Rab5-positive and Rabankyrin-5-positive vesicles (all measured at greater than 1 μm in diameter) – these proteins are two well-established markers of macropinosomes (Mettlen et al., 2006; Schnatwinkel et al., 2004). Compared to control cells, in which 46% of cells contained macropinosomes (Fig. 4D–F, see insets, quantified in 4J), after 20 min of PDGF stimulation only 10% of MICAL-L1-KD cells had macropinosomes (Fig. 4G–I, quantified in Fig. 4J). Given that Src activation at the periphery is required for CDR formation in mouse fibroblasts (Azimifar et al., 2012), it is interesting that CDRs form in MICAL-L1-KD cells at similar rates to those observed in control cells. However, by using live-cell imaging, we found that the CDRs in MICAL-L1-KD cells displayed altered morphology (data not shown) and that MICAL-L1 KD clearly affected CDR maturation into macropinosomes (Fig. 4D–I). Thus, MICAL-L1 might also directly affect CDR maturation in addition to its function in trafficking Src to PDGF-induced CDRs in human fibroblasts.

MICAL-L1 is required for PDGF-induced focal adhesion turnover

Recent studies have demonstrated that integrins and other focal adhesion proteins (such as paxillin and FAK, Fig. 3) rapidly

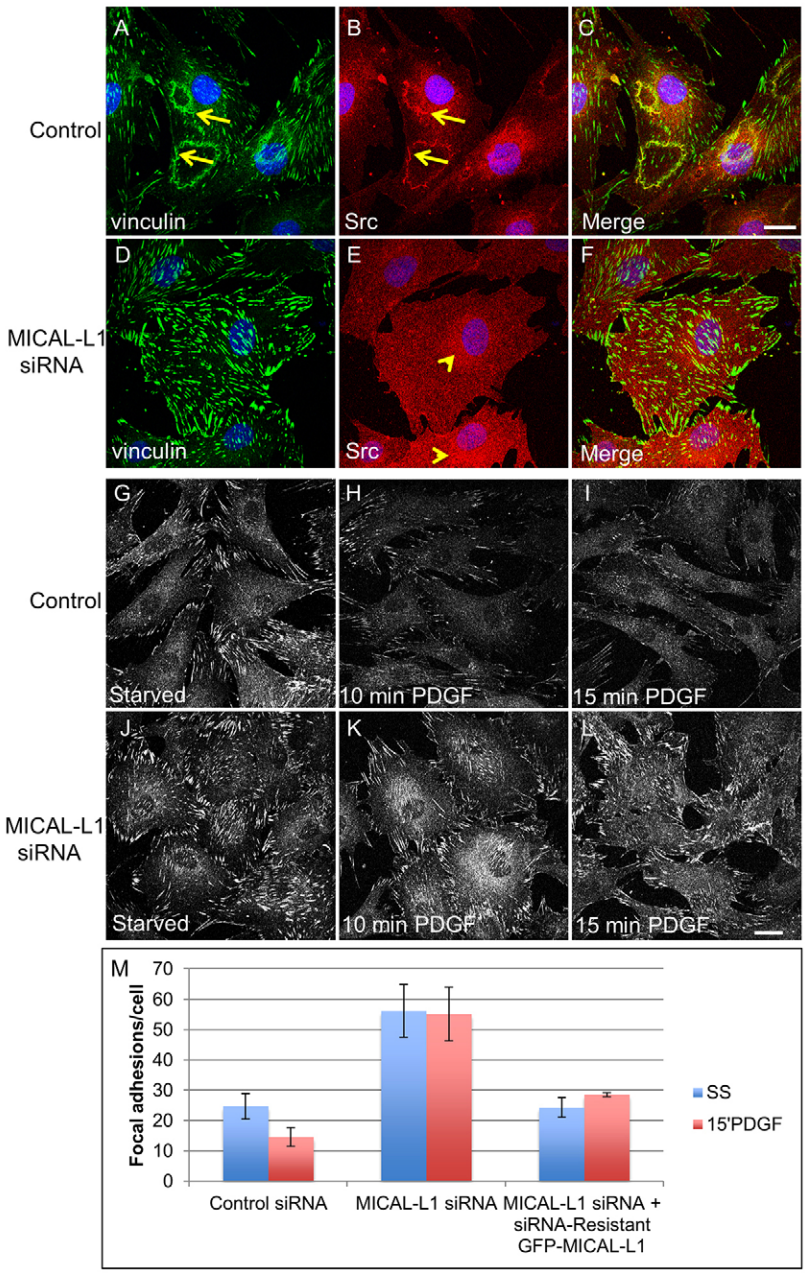

Fig. 5. MICAL-L1 regulates PDGF-induced focal adhesion turnover. (A–F) Representative images of control and MICAL-L1-depleted fibroblasts stimulated with PDGF for 10 min and stained for vinculin (green) and Src (red). Arrows denote the colocalization of Src and vinculin at CDRs in control cells, whereas arrowheads mark the ERC-localized Src in MICAL-L1-depleted cells. (G–L) Control and MICAL-L1-depleted fibroblasts were serum-starved (SS) (G,J) or stimulated with PDGF for 10 min (H,K) or 15 min (I,L). Focal adhesions are labeled with vinculin. (M) The number of focal adhesions in SS or PDGF-stimulated cells was quantified using ImageJ. Error bars show s.e.m. from three independent experiments. The total number of cells and focal adhesions are shown in Fig. 6E. For rescue, focal adhesions were quantified from 45 cells from three independent experiments (15 per experiment). The Tukey test was used to calculate the statistical significance between treatments. The number of focal adhesions was significantly different ($P<0.01$) between control serum-starved and MICAL-L1-KD serum-starved cells but not between control and MICAL-L1-rescue SS cells. There was also a significant difference between control cells treated with PDGF and MICAL-L1-depleted cells treated with PDGF. MICAL-L1-rescue cells treated with PDGF had significantly fewer focal adhesions than MICAL-L1-KD cells under similar conditions, but the number was also significantly different from control cells treated with PDGF ($P<0.05$). Blue, DNA stained with DAPI. Scale bars: 10 μm.

Journal of Cell Science (2014) 127, 1684–1698 doi:10.1242/jcs.133892

redistribute to CDRs upon PDGF stimulation and that this redistribution is linked to focal adhesion turnover and cell migration (Gu et al., 2011; Hoon et al., 2012). We first addressed whether MICAL-L1 KD in human fibroblasts affected focal adhesions at steady state. MICAL-L1 was easily depleted in these cells with a range of different concentrations of siRNA (supplementary material Fig. S2A). A modest reduction in Src-pY419 was observed in MICAL-L1-KD cells, with little or no impact on FAK-pY397, paxillin-pY118 or actin (supplementary material Fig. S2A). MICAL-L1-depleted BJ cells displayed larger more-prominent focal adhesions under steady-state conditions (compare supplementary material Fig. S2E to S2D for vinculin and Fig. S2G to S2F for paxillin). Furthermore, active Src was largely absent from focal adhesions in MICAL-L1-depleted cells (compare supplementary material Fig. S2C to S2B), suggesting that focal adhesion dynamics might be impaired because of the lack of recruitment of active Src. Because the kinase activity of Src is required for focal adhesion turnover (Fincham and Frame, 1998), we hypothesized that the loss of MICAL-L1 might impair PDGF-induced focal adhesion turnover in BJ cells.

Following PDGF stimulation, Src and the focal adhesion protein vinculin colocalized along CDRs in control cells (Fig. 5A–C, arrows). This result agreed with findings from our laboratory and from other laboratories that focal adhesion proteins redistribute to CDRs in response to growth factor stimulation. However, MICAL-L1 depletion caused considerable retention of Src in the perinuclear region (Fig. 5E, arrowheads) and impaired the re-distribution of vinculin to CDRs (Fig. 5D). Control and MICAL-L1-KD cells both formed actin-positive CDRs (supplementary material Fig. S3B,E, yellow arrows), thus the failure of vinculin to localize to CDRs (supplementary

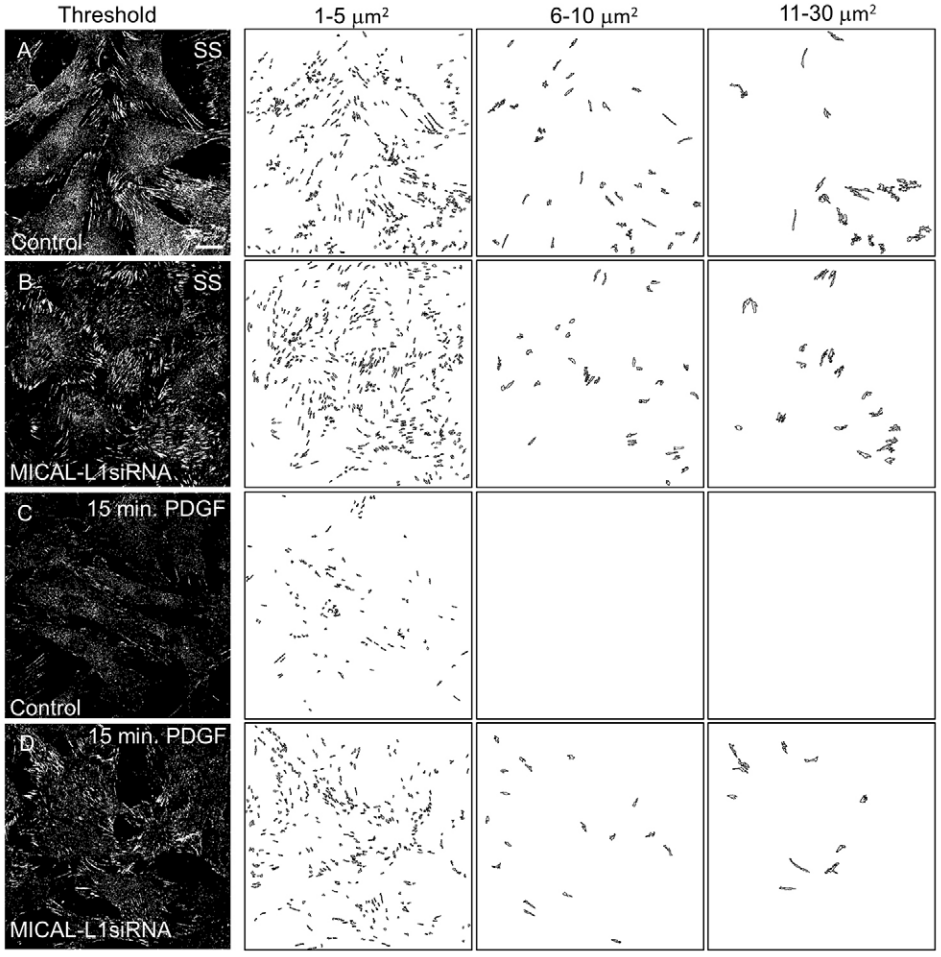

E

Focal Adhesion Area	Control SS	MICAL-L1 SS	Control 15'PDGF	MICAL-L1 15'PDGF
1-5 μm²	93.5	88.1	97.5	89.8
6-10 μm²	4.7	7.9	1.6	6.9
11-30 μm²	1.8	4.0	1.0	3.3
Total focal adhesions	4540.0	8853.0	1176.0	5356.0
Total number of cells	184.0	161.0	122.0	100.0

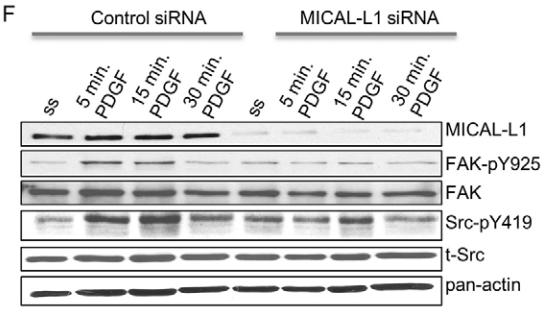

Fig. 6. MICAL-L1 depletion impedes focal adhesion turnover and leads to increased focal adhesion size. (A–D) Images from Fig. 5 were used to demonstrate the size-distribution quantification of focal adhesions in control and MICAL-L1-depleted BJ cells. Images were imported into ImageJ and fluorescence levels were set to a threshold to optimally depict focal adhesions. Focal adhesion area was calculated using the 'measure particles' function, and size distributions were set to group focal adhesions into three size categories: small (1–5 μm^2), medium (6–10 μm^2) and large (11–30 μm^2). (E) A summary of focal adhesion number and size distribution in serum starved (SS) and PDGF-stimulated cells. Data are presented as the percentage of focal adhesions within each area category for three independent experiments. The Tukey test was used to calculate statistical significance. For small focal adhesions, there were significantly fewer focal adhesions in PDGF-treated MICAL-L1-KD cells compared to control. By contrast, MICAL-L1-KD cells had significantly more medium and large focal adhesions compared to control cells ($P<0.01$). (F) A representative immunoblot of BJ cells stimulated with PDGF in the presence (lanes 1–4) or absence of MICAL-L1 (lanes 5–8). FAK, total Src (t-Src) and actin were used as loading controls. Scale bar: 10 μm.

Journal of Cell Science (2014) 127, 1684–1698 doi:10.1242/jcs.133892

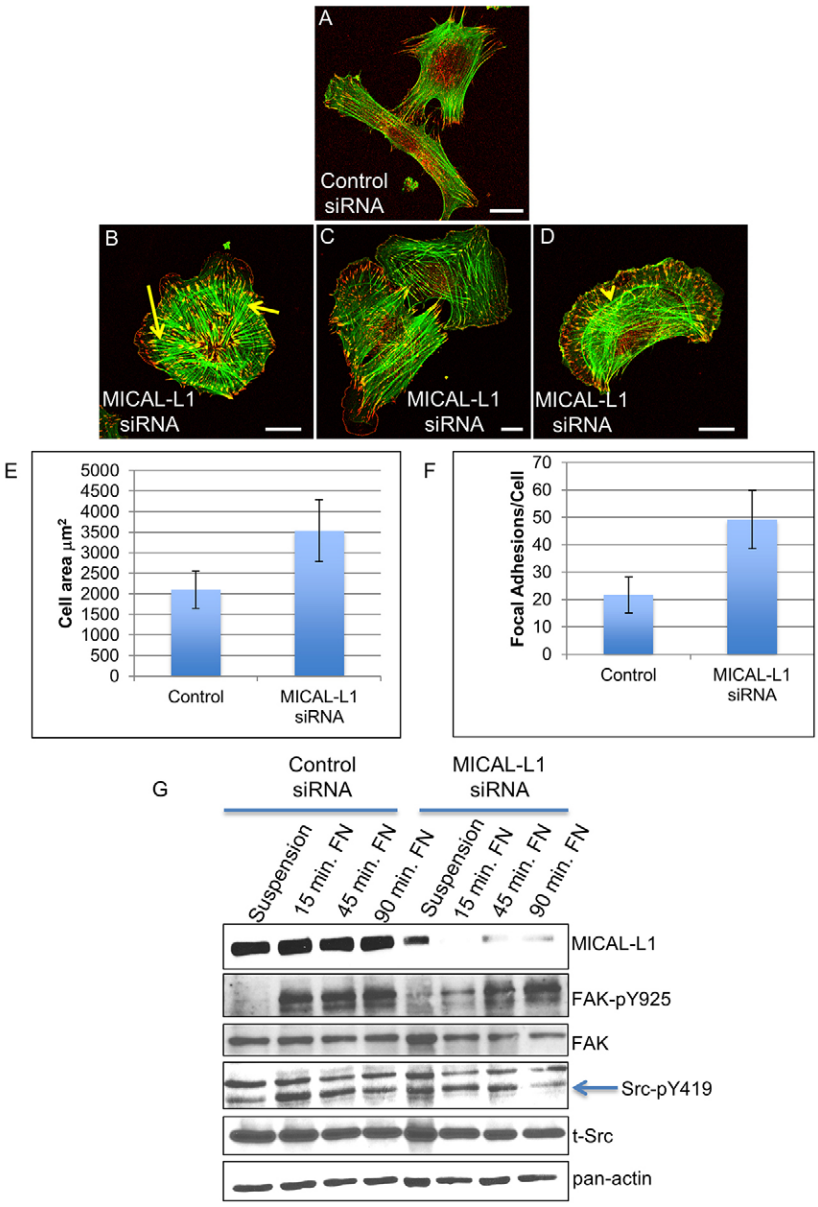

Fig. 7. MICAL-L1 is required for normal cell spreading on fibronectin and optimal integrin-induced Src activation. (A–D) Control (A) and MICAL-L1-depleted cells (B–D) were serum starved (SS) in suspension for 1 h and then plated onto 10 µg/ml fibronectin-coated coverslips for 90 min and stained with phalloidin-488 (green) and anti-vinculin (red). During spreading of MICAL-L1-depleted cells, prominent short actin cables (B, arrows), polygonal cells with disorganized actin stress fibers (C) and dorsal actin arcs (D, arrowhead) were observed. Scale bars: 10 µm. (E) The cell area (mean±s.e.m.) was quantified from three independent experiments (control $n=65$, MICAL-L1 siRNA $n=66$) using Pascal LSM Image Examiner. One-way ANOVA demonstrated a significant increase in the area of MICAL-L1-KD cells compared to control cells ($P<0.01$). (F) The mean number of focal adhesions per cell was quantified from three independent experiments (control, $n=40$; MICAL-L1 siRNA, $n=53$). There were significantly more focal adhesions per cell in MICAL-L1 KD cells ($P<0.01$). (G) A representative immunoblot of BJ cells held in suspension or plated onto fibronectin-coated plates in the presence (lanes 1–4) or absence of MICAL-L1 (lanes 5–8). The arrow denotes the Src band. FAK, total Src (t-Src) and actin were used as loading controls.

material Fig. S3A,D) is not because CDRs do not form in MICAL-L1-KD cells. MICAL-L1-depleted cells displayed increased vinculin-positive focal adhesions (Fig. 5D) compared to control cells. To test whether MICAL-L1-depletion impaired focal adhesion turnover, which would explain the increased number of focal adhesions, we quantified the number of focal adhesions in PDGF-stimulated cells. As shown in Fig. 5G–I and quantified in Fig. 5M, cells that were treated with control siRNA displayed a significant time-dependent decrease in the number of vinculin-containing focal adhesions (serum starved, 24.6±4.1; 15-min PDGF treatment, 14.5±3.1; means±s.e.m.). Under non-stimulated conditions, MICAL-L1 depletion caused a significant increase in the number of focal adhesions per cell (serum starved, 56.2±8.7) relative to control (Fig. 5J,M). Moreover, stimulation of MICAL-L1-depleted cells did not lead to focal adhesion disassembly (PDGF, 55.1±8.8). The re-introduction of MICAL-L1 into MICAL-L1-depleted cells partially rescued the increase in focal adhesion number (serum starved, 24.3±3.3; PDGF, 28.4±0.71; quantified in Fig. 5M with representative images in supplementary material Fig. S3G–J). Furthermore, the re-introduction of MICAL-L1 to MICAL-L1-KD cells partially rescued PDGF-induced cellular elongation, a phenotypic marker that we used to assess cell migration in fixed cells (supplementary material Fig. S4).

To further address the impact of MICAL-L1 depletion on focal adhesion stability, we quantified the size of focal adhesions, as this is linked to impaired turnover (Webb et al., 2004). Focal adhesion size in BJ cells was categorized into three pools: small (1–5 µm^2), medium (6–10 µm^2) and large (11–30 µm^2). Fig. 6A–D are representative examples of fields of cells from Fig. 5 where this has been quantified (Fig. 6A corresponds to Fig. 5G, Fig. 6B to Fig. 5J, Fig. 6C to Fig. 5I and Fig. 6D to Fig. 5L). PDGF stimulation of control BJ cells (Fig. 6C) caused the disassembly of the larger focal adhesions that are present under serum-starved conditions (Fig. 6A). The distribution of focal adhesion size in serum-starved and MICAL-L1-KD cells before and after PDGF stimulation (for 15 min) is shown in the form of a table (Fig. 6E). The majority of focal adhesions in

Journal of Cell Science (2014) 127, 1684–1698 doi:10.1242/jcs.133892

control cells are between 1 and 5 μm^2 (serum starved, 93.5%; PDGF, 97.5%). By contrast, MICAL-L1 depletion led to a decrease in the population of small focal adhesions (88.1%) that does not change substantially following PDGF stimulation (89.8%).

Although there are many Src substrates present at focal adhesions, FAK phosphorylation at position Y925 is crucial for focal adhesion turnover (Deramaudt et al., 2011). We hypothesized that phosphorylation of FAK-Y925 would be impaired if Src activity was decreased at focal adhesions in MICAL-L1-depleted cells. BJ cells were stimulated with PDGF and immunoblots were used to measure FAK-pY925. In control cells, there was a sharp increase in Y925 phosphorylation following PDGF stimulation for 5 or 15 min (Fig. 6F, lanes 1–4). This rise in phosphorylation coincided with increased levels of active Src. However, MICAL-L1-depleted cells displayed impaired PDGF-induced activation of Src (lanes 5–8). Consequently, no increase in FAK-pY925 was observed. These data reinforce the hypothesis that MICAL-L1 regulates the transport of active Src to focal adhesions, thus controlling the turnover of focal adhesions.

MICAL-L1 regulates cell spreading

Adhesion molecules, such as integrin receptors, mediate cell attachment to the extracellular matrix. Upon attachment, cell spreading requires the continual formation and disassembly of focal adhesions, and Src is crucial for this process (Huveneers and Danen, 2009). To test whether MICAL-L1 is required for the spreading of BJ cells, cells that were treated with control siRNA or siRNA specific to MICAL-L1 were plated onto fibronectin-coated coverslips for 90 min. Control cells spread and polarized, displaying long actin stress fibers with vinculin-positive focal adhesions localized at the cell periphery at the end of these stress fibers (Fig. 7A).

By contrast, MICAL-L1-depleted cells failed to polarize on fibronectin-coated coverslips (Fig. 7B–D). We observed several abnormal phenotypes in these cells, including large round cells with prominent actin cables distributed throughout the cell

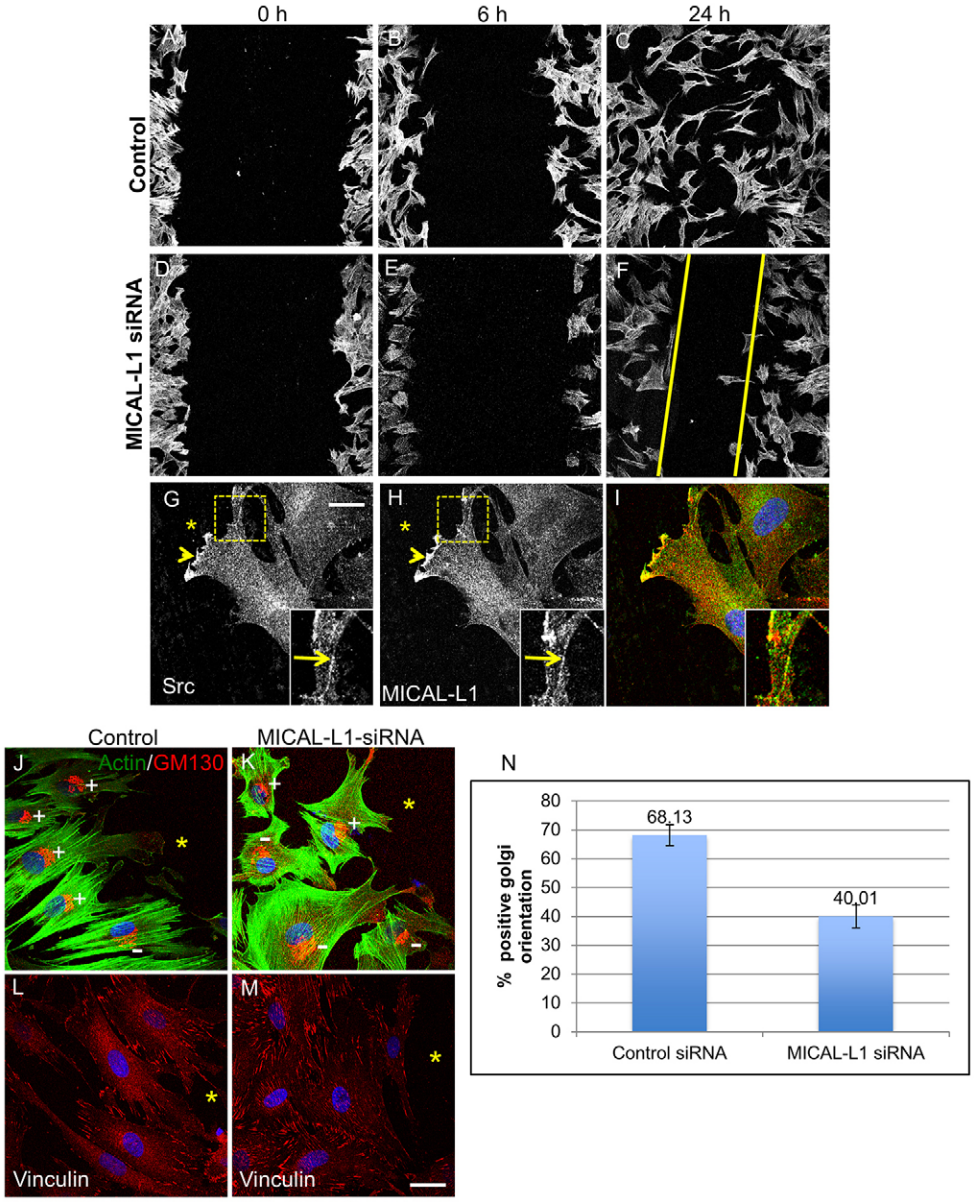

Fig. 8. MICAL-L1 is required for cell migration. (A–F) BJ cells were grown to confluence on fibronectin-coated coverslips and a scratch wound was created. Monolayers were washed and incubated in low-serum medium for the times indicated, and then were fixed and stained with phalloidin. Images were taken with a 10× objective and are representative of three independent experiments. The yellow line denotes the final degree of wound closure. (G–I) Cells were wounded, allowed to migrate for 6 h and then stained for Src (G) and MICAL-L1 (H). The arrowhead marks colocalization along the leading edge. Arrows in the inset show colocalization along tubulo-vesicular structures. (J–N) Loss of MICAL-L1 impairs wound polarization. Cell monolayers were wounded and allowed to migrate for 6 h prior to fixation and were then stained with phalloidin and anti-GM130 (J,K) or anti-vinculin (L,M). + and − denote proper polarization of the Golgi apparatus towards the wound, or lack of it, respectively. Representative images of three independent experiments are shown (J–M) and quantified (N, statistically significant, $P<0.05$, error bars show s.e.m.). The asterisk shows the location of the wound. Blue, DNA stained with DAPI. Scale bars: 10 μm.

Journal of Cell Science (2014) 127, 1684–1698 doi:10.1242/jcs.133892

(Fig. 7B, arrows), polygonal cells with disorganized actin stress fibers (Fig. 7C), and cells with a single broad lamellipodium containing actin arcs (Fig. 7D, arrowhead). MICAL-L1-depleted cells were also larger (3537 $\mu m^2 \pm 754$, means±s.e.m.) than control cells (2098 $\mu m^2 \pm 455$) and contained more focal adhesions per cell (MICAL-L1 depleted, 49.2±10.7; control, 21.6±6.6, see Fig. 7E,F).

Having established that MICAL-L1 is required for normal BJ cell spreading, we tested whether integrin-induced Src activation was affected by MICAL-L1 depletion. When control BJ cells were plated onto fibronectin, Src activation increased compared to cells held in suspension (Fig. 7G, lanes 1–4). MICAL-L1 deficiency caused a modest decrease in Src activation upon fibronectin plating (Fig. 7G, lanes 5–8, arrow), as shown by the decreased levels and delayed appearance of FAK-pY925 (Fig. 7G, lanes 5–8) compared to control cells. A reduction in Src activation and in Src-dependent phosphorylation of FAK is consistent with the impaired focal adhesion turnover that we observed during cell spreading (Fig. 7B–D).

MICAL-L1 depletion affects directional cell migration

Because focal adhesion turnover and spreading are both necessary for cell migration, we hypothesized that MICAL-L1 might be a regulator of cell migration. To test this idea, we performed scratch-wound assays using control cells and MICAL-L1-depleted cells. BJ cells migrated into the wound within 24 h (Fig. 8A–C). In comparison, MICAL-L1-depleted cells were impaired in wound closure (Fig. 8D–F). Src and MICAL-L1 colocalized along the leading edge (Fig. 8G,H, arrowhead) and along tubules at the cell front (Fig. 8G,H, inset and arrow) of migrating cells. Because Src is required for the polarization of the cell to the wound (Magdalena et al., 2003; Timpson et al., 2001), we assessed polarity in migrating fibroblasts using the orientation of the Golgi complex and the actin cytoskeleton as well-established markers of polarization. Although the majority of control cells displayed Golgi that were oriented to the wound and stress fibers that were perpendicular to the wound (Fig. 8J, quantified in 8N, 68%), MICAL-L1-depleted cells were partially impaired in their ability to polarize to the wound (Fig. 8K, quantified in 8N, 40%).

Cell migration requires the formation and disassembly of focal adhesions at the cell front and the disassembly of focal adhesions at the cell rear (Wozniak et al., 2004). In control cells, there were increased numbers of focal adhesions as well as an increased intensity of vinculin staining at the cell front compared to the dimmer less-frequent staining at the cell rear (Fig. 8L). In comparison, MICAL-L1-depleted cells displayed an overall increase in the number of focal adhesions (in agreement with our previous data) but failed to polarize in the direction of the wound (Fig. 8M). Taken together, these results demonstrate the requirement of MICAL-L1 for polarized cell migration in BJ cells.

EHD1 is required for Src transport and activation and acts as a molecular 'pinchase' on MICAL-L1 tubules to release Src from the ERC in response to EGF

Having established that MICAL-L1 colocalizes with Src and regulates its trafficking and activation in response to a variety of stimuli, we sought to understand the mechanism by which MICAL-L1 regulates Src. In the absence of a direct interaction between the two proteins, we postulated that MICAL-L1 regulates the release of Src from the ERC and its subsequent activation by recruiting vesiculating proteins such as EHD1. This hypothesis is further strengthened by the fact that we have previously shown that EHD1 also regulates focal adhesion turnover and cell migration in fibroblasts (Jović et al., 2007); however, the mechanism by which this occurs remains unclear. We hypothesized that impaired Src recruitment to focal adhesions could explain these deficits. Indeed, EHD1 KD in HeLa cells led

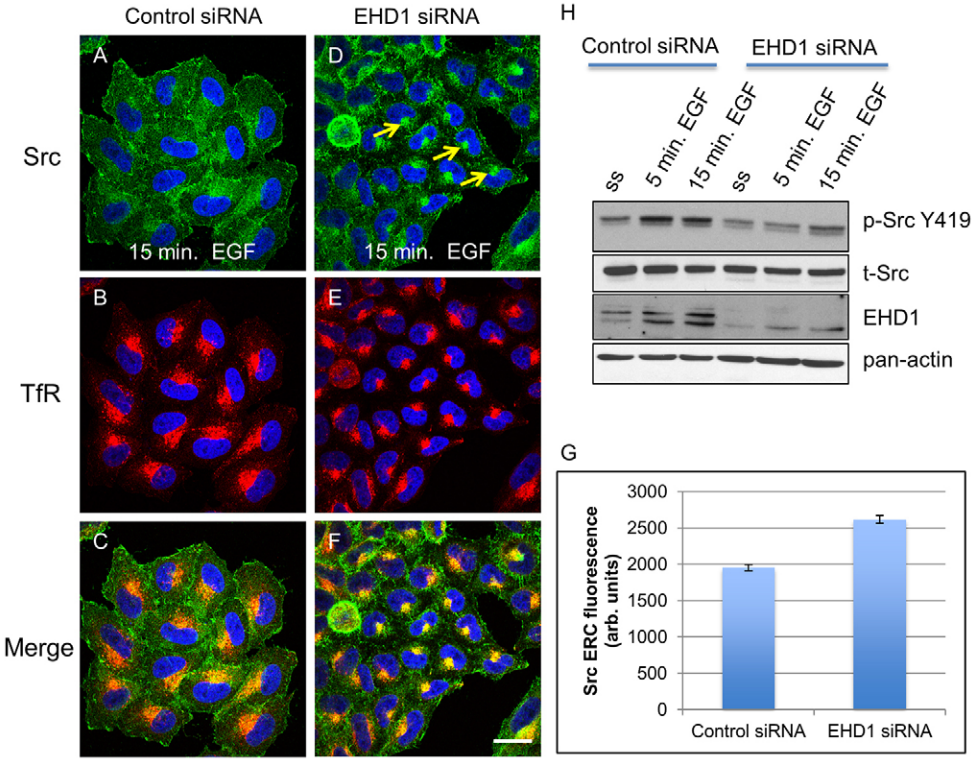

Fig. 9. EHD1 is required for EGF-induced Src translocation and activation in HeLa cells. Control cells (A–C) and EHD1-siRNA-treated cells (D–F) were stimulated with EGF and stained with Src (green) and TfR (red). Treatment with EHD1 siRNA results in the retention of Src in the ERC (overlap between Src and TfR, compare C to F). (G) The level of Src fluorescence in the ERC was quantified from three independent experiments and found to be significantly higher in EHD1-KD cells (one-way ANOVA, $P<0.01$). (H) An immunoblot demonstrating impaired Src activation in EHD1-depleted cells (lanes 4–6) compared to control cells (lanes 1–3). Actin and total Src (t-Src) were used as loading controls. SS, serum starved. Error bars show s.e.m. Blue, DNA stained with DAPI. Scale bar: 10 μm.

Journal of Cell Science (2014) 127, 1684–1698 doi:10.1242/jcs.133892

to a significant retention of Src in the TfR-positive ERC (Fig. 9A–F, see arrows in 9D; quantified in 9G). In addition, EHD1 KD impaired EGF-induced Src activation (Fig. 9H, compare control lanes 1–3 to EHD1 KD lanes 4–6).

We have recently shown that MICAL-L1 is a regulator of recycling tubule biogenesis in HeLa cells (Giridharan et al., 2013). Interestingly, MICAL-L1 might also facilitate the cleavage or vesiculation of recycling tubules by recruiting molecular 'pinchases' such as EHD1 (Cai et al., 2013). Whether MICAL-L1 and EHD1 constitutively bind to one another in cells, or whether EHD1 is recruited to MICAL-L1 by certain stimuli, remains unclear. Therefore, we tested whether EGF stimulation in HeLa cells affected the subcellular localization of EHD1 or MICAL-L1. Under steady-state conditions, EHD1 was concentrated in the perinuclear region (Fig. 10A) but was also found on a subset of MICAL-L1-positive tubules. MICAL-L1 was also concentrated in the perinuclear region; however, MICAL-L1-positive tubules emanating from the ERC were also visible (Fig. 10B), with many being EHD1 negative. Serum starvation resulted in the displacement of EHD1 from the ERC (Fig. 10D), and a modest increase in MICAL-L1 tubulation and in the spreading of the tubular endosomes out of the ERC (Fig. 10E). Surprisingly, EGF stimulation had dramatic effects on MICAL-L1-decorated tubular recycling endosomes and EHD1 localization. Firstly, MICAL-L1-positive tubules were substantially shortened and were displaced to the cell periphery (Fig. 10H, see arrows). Secondly, in contrast to serum-starved cells, EGF induced an apparent increase in the extent to which EHD1 was concentrated at MICAL-L1-positive tubular structures (Fig. 10G, arrows), suggesting that EGF might either enhance the recruitment of

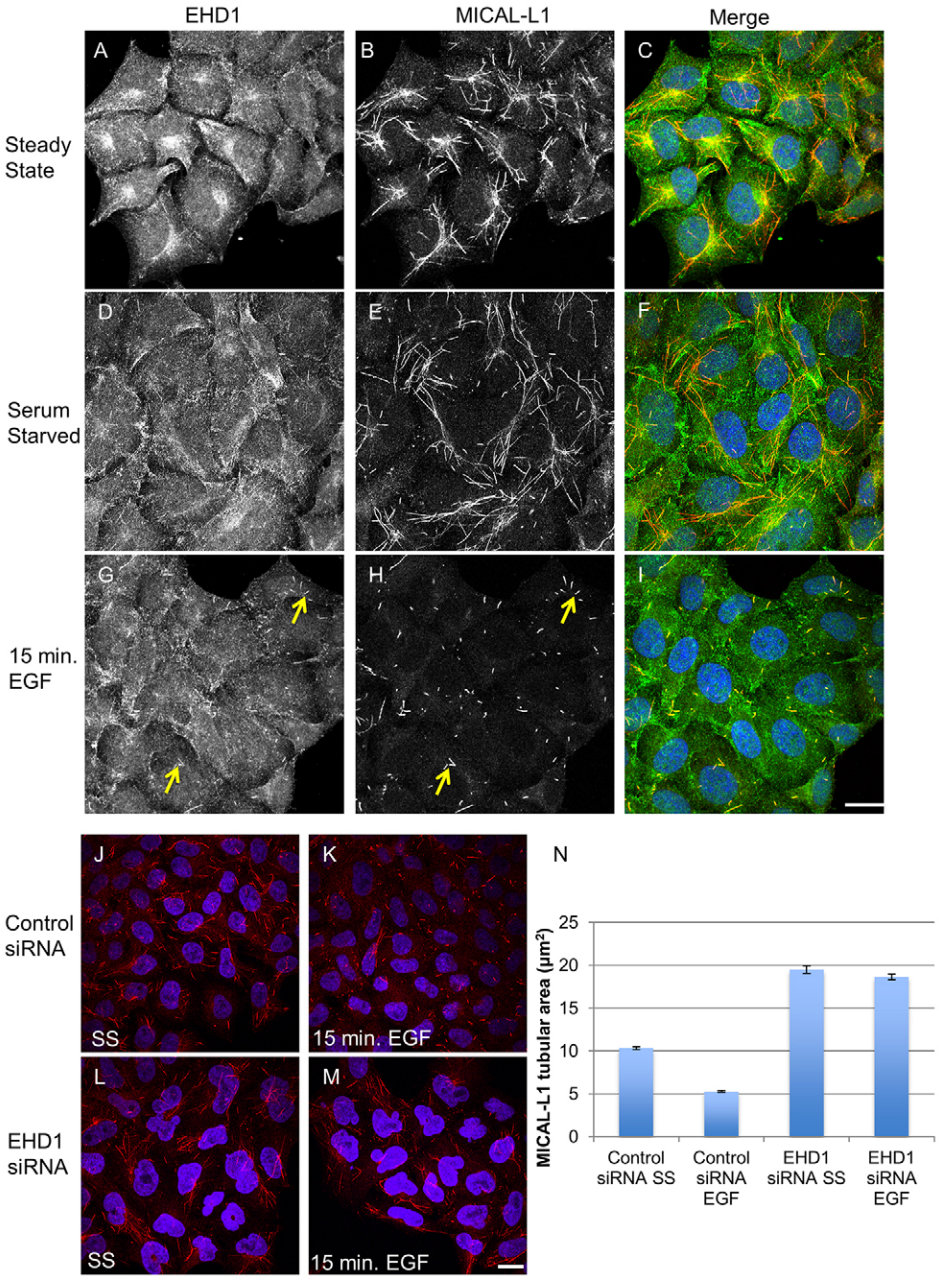

Fig. 10. EHD1 is required for EGF-induced MICAL-L1-positive tubule vesiculation. (A–I) Compared to cells in the steady state (A–C) and serum-starved cells (SS) (D–F), EGF treatment (G–I) induces increased recruitment of EHD1 to MICAL-L1-positive tubules (arrows) resulting in the cleavage and vesiculation of MICAL-L1-decorated recycling tubules. (J–N) Treatment with EHD1 siRNA impairs the vesiculation of MICAL-L1-decorated tubular endosomes in response to EGF. In control cells, EGF stimulation leads to a reduction in the total area of MICAL-L1-containing tubular endosomes (compare K to J, quantified in N). Treatment with EHD1 siRNA results in a modest increase in the area of MICAL-L1-containing tubular endosomes in SS cells (L). In the absence of EHD1, EGF stimulation does not induce vesiculation of MICAL-L1-decorated tubular endosomes (M, quantified in N). Tubule area was quantified from three independent experiments (at least 30 cells per experiment). A Tukey test demonstrated that there were significant increases in the area of MICAL-L1-positive tubules in SS and EGF-treated EHD1-KD cells compared to control ($P<0.01$). No significant difference was observed between SS EHD1-KD and EGF-treated EHD1-KD cells. Error bars show s.e.m. Blue, DNA stained with DAPI. Scale bars: 10 μm.

Journal of Cell Science

EHD1 to tubules or possibly stimulate the ATPase activity of EHD1, leading to the vesiculation of MICAL-L1-containing tubular recycling endosomes.

Although the molecular mechanisms governing the increased recruitment of EHD1 to MICAL-L1-positive tubules in response to EGF are unclear, the fact that EGF induced dramatic changes to MICAL-L1 recycling tubules was unexpected, and it suggested that the release of Src from the ERC in response to EGF might be mediated by the recruitment of EHD1. Therefore, we tested whether the EGF-induced vesiculation of MICAL-L1-positive tubules was dependent on EHD1. Similar to our previous experiments, EGF stimulation led to dramatic shortening, peripheral scattering and reduction of MICAL-L1-positive tubules compared to serum-starved control cells (compare Fig. 10K to 10J, quantified in 10N). By contrast, EHD1 KD resulted in a modest increase in MICAL-L1-positive tubular area under serum-starved conditions (Fig. 10L) that did not decrease with EGF stimulation (Fig. 10M, quantified in 10N). In summary, we conclude that MICAL-L1 and EHD1 regulate Src trafficking and activation. MICAL-L1 recruits EHD1 to perinuclear ERC endosomes, allowing for the release of Src from the ERC and its transportation to the plasma membrane, where Src functions in mediating the rearrangement of the actin cytoskeletal (CDR), focal adhesion disassembly and cell migration (Fig. 11, see model).

DISCUSSION

Cell adhesion and migration requires the correct spatiotemporal activation of many kinases, phosphatases and GTPases, with the kinase Src being central to the entire process (Huveneers and Danen, 2009). Insufficient Src activation paralyzes the cell and prevents the turnover of focal adhesions (Fincham and Frame, 1998), whereas excessive Src activation can promote the spreading of cancer cells, invasion and metastasis (Wheeler et al., 2009). Accordingly, exquisite regulation of Src activity is paramount to normal cell behavior.

We found that Src localizes to MICAL-L1-positive tubular recycling endosomes in HeLa cells (Fig. 1) and that MICAL-L1 and its binding partner EHD1 are required for stimulation-induced Src transport and activation (Figs 2, 9). HeLa cells have an extensive network of recycling tubules, potentially because of different expression of individual EHD proteins and/or a slow rate of ATP hydrolysis and fission, and are thus a useful tool for studying recycling. In other cells, including fibroblasts, the morphology of the ERC is less compact, more dispersed and harder to visualize. However, we also investigated the localization of Src and MICAL-L1 in human fibroblasts (Fig. 3). Although some MICAL-L1 and Src can be detected on tubular recycling endosomes in these cells, we were surprised to find that in addition to small, presumably lipid-rich tubular structures (data not shown), MICAL-L1 localized to PDGF-stimulated actin-rich CDRs, where it colocalized with Src. Because normal fibroblasts are an excellent model to study CDRs and focal adhesions, we used the two cell lines intermittently to study the regulation of Src by MICAL-L1. Overall, the fact that MICAL-L1 colocalized with Src in human fibroblasts and was crucial for Src recruitment and activation (Figs 4, 6) was consistent with our data in HeLa cells, allowing us to conclude that the regulation of Src localization and activity by MICAL-L1 is general and not specific to one cell type.

Although our data provide new information regarding the regulation of Src transport out of the ERC (Fig. 11, ERC-to-plasma membrane pathway), they do not address the other arm of the Src endocytic regulatory pathway (Fig. 11, plasma membrane-to-ERC pathway). How a stimulus (such as EGF) at the cell surface is able to promote the movement and activation of an intracellular protein that is localized to the ERC remains unknown. Sandilands and Frame proposed a novel mechanism in which a small pool of Src localizes to the plasma membrane, even in the absence of stimulus (Sandilands and Frame, 2008). Upon stimulation with growth factor or integrin activation, this small pool of plasma-membrane Src is activated, whereby it translocates to the ERC (Fig. 11, blue dashed arrow). This would initiate a positive-feedback loop to activate the larger pool of ERC-localized Src. One phenomenon that we commonly observed was that cells depleted of MICAL-L1 or EHD1 had relatively more active Src under serum-starved conditions

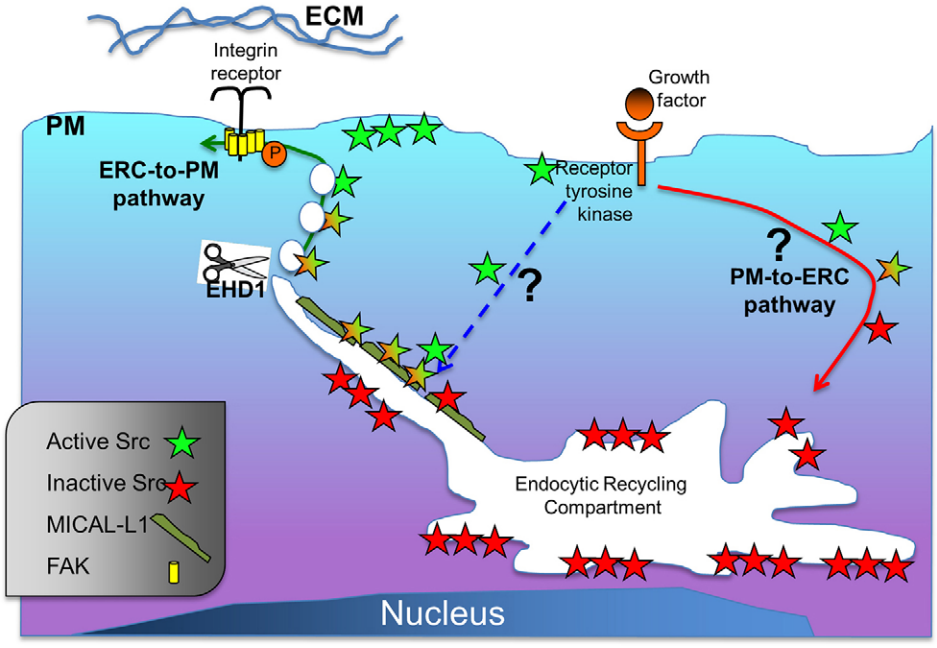

Fig. 11. Schematic model depicting the proposed roles of MICAL-L1 and EHD1 in mediating Src translocation from the ERC to the plasma membrane in response to growth factor or integrin stimulation. Inactivated Src is maintained at the ERC. Upon growth factor receptor stimulation (i.e. EGF), Src is sorted into MICAL-L1-decorated tubular recycling endosomes and becomes partially activated by an unknown mechanism. EHD1 is recruited to the tubular recycling endosomes by MICAL-L1, where it vesiculates recycling endosomes that contain Src and are transported to the plasma membrane where Src becomes fully activated.

compared to serum-starved control cells or MICAL-L1-KD and EHD1-KD cells that were stimulated with growth factor (refer to immunoblots in Figs 2, 6, 7 and 9). This lends support to the idea that the loss of MICAL-L1 or EHD1 might trap a relatively larger pool of Src at the plasma membrane under serum-starved conditions (compared to control cells).

Accordingly, it is possible that MICAL-L1 and EHD1 also play a role in in the plasma membrane–ERC pathway (Fig. 11), as MICAL-L1 also regulates the transport of some receptors into the perinuclear ERC by its interaction with the collapsin response mediator protein-2 (CRMP2, also known as DPYSL2) and dynein, which modulate microtubule-based transport (Rahajeng et al., 2010). Interestingly, the localization of Src to the ERC is microtubule dependent (Fincham et al., 2000). Indeed, nocodazole-induced disruption of microtubules stabilizes focal adhesions, whereas nocodazole washout promotes the synchronous disassembly of focal adhesions (Ezratty et al., 2005). We speculate that the re-establishment of the microtubule network promotes Src transport into the ERC, activation of Src and its subsequent transport to the plasma membrane for the disassembly of focal adhesions. Future studies will be needed to dissect the specific contribution of microtubules and microtubule motor proteins to Src activation, and to understand how this regulates microtubule-induced focal adhesion turnover.

Finally, we found that MICAL-L1-positive recycling tubules (in HeLa cells) are highly dynamic. Specifically, EGF stimulation induced a rapid shortening of MICAL-L1-positive tubules (Fig. 10). The molecular mechanisms regulating this phenomenon remain enigmatic; however, our data clearly implicate EHD1 in mediating EGF-induced MICAL-L1 vesiculation. Although EHD1 and other EHD family members are phosphorylated in response to serum (Fichtman et al., 2008), it is unclear what effect phosphorylation or other potential post-translational modifications have on the ATPase activity of EHD proteins or on their recruitment to endocytic membranes.

Our data clearly demonstrate the importance of MICAL-L1 and EHD1 in regulating both the transport of Src from the ERC to the plasma membrane and Src activation. The finding that MICAL-L1 depletion affects Src-dependent processes such as focal adhesion dynamics, adhesion and migration underscores the *in vivo* relevance of tubular endosomes that contain both Src and MICAL-L1, and highlights the potential significance of MICAL-L1 and EHD1 in regulating non-receptor kinases.

MATERIALS AND METHODS

Reagents and antibodies

Recombinant human PDGF-BB, EGF and EGF–Rhodamine were purchased from Invitrogen. Fibronectin was purchased from Sigma. Antibodies against the following proteins were used: EHD1 (Caplan et al., 2002); vinculin (Sigma); GM130 (BD Biosciences); Rab5 (Abcam); Rabankyrin-5 (Abnova); Src (36D10), phospho-Src (tyrosine 416, D49G4), FAK, phospho-FAK (tyrosine 925), EGFR and phospho-FAK (tyrosine 1068, all from Cell Signaling Technologies); phospho-FAK (tyrosine 397) and phospho-paxillin (tyrosine 118, both from Invitrogen); actin and MICAL-L1 (both from Novus); phospho-Src (tyrosine 416, used for immunofluorescence, Millipore); and human transferrin receptor (Zymed).

Cell culture

The HeLa cervical cancer cell line (ATCC-CCL2) and SYF mouse embryonic fibroblasts [ATCC-CRL2459 (Klinghoffer et al., 1999)] were grown in DMEM (high glucose) containing 10% fetal bovine serum (FBS), 1× penicillin-streptomycin (Invitrogen) and 2 mM glutamine. Normal human foreskin fibroblasts (BJ, ATCC-2522) were grown in EMEM containing 10% FBS, 1× penicillin-streptomycin, 2 mM glutamine and 1× non-essential amino acids.

Plasmids, siRNA transfections and rescue experiments

Human Src–GFP was created similarly to as described previously (Sandilands et al., 2004). Briefly, human Src (Invitrogen, IOH12563) was amplified by PCR using the forward primer 5′-CCGCTCGAGAT-GGGTAGCAACAAGAGCAAGCC-3′ and the reverse primer 5′-CC-CAAGCTTTGATCCTGATCCGAGGTTCTCCCCGGGCTGG-3′. The resulting PCR product, which contains (from 5′ to 3′) a 5′ *Xho*I restriction site, the Src ORF, a Gly-Ser-Gly-Ser linker and a 3′ *Hind*III site, was ligated into pre-digested EGFP-N1 plasmid (Clontech) and verified by sequencing. HA–MICAL-L1 was as described previously (Sharma et al., 2009). Plasmids were transfected into SYF cells using FuGene HD (Roche).

Pooled and individual oligonucleotides targeting human MICAL-L1, custom EHD1 siRNA (Sharma et al., 2009) and non-targeting control siRNA were obtained from Dharmacon. HeLa cells were transfected by using Oligofectamine (Invitrogen) with 150 nM siRNA, whereas BJ cells were transfected by using Lipofectamine RNAiMAX (Invitrogen) with 50 nM siRNA. The efficiency of protein knockdown was measured at 48–72 h post-transfection by immunoblotting or immunofluorescence for each experiment. For rescue experiments, 8×10^5 BJ cells were electroporated at 48 h post-transfection, by using Amaxa Nucleofector II according to the manufacturer's protocol with an siRNA-resistant GFP–MICAL-L1 construct.

Growth factor stimulation and phenotype analysis

Cells grown on glass coverslips (HeLa) or on 10 µg/ml fibronectin-coated coverslips (BJ) were serum starved overnight (18 h) in Opti-MEM medium. Cells were then stimulated with EGF (50 ng/ml) or PDGF (15 ng/ml) for the times indicated prior to immunoblotting or immunofluorescence.

Src ERC fluorescence was measured using ImageJ. Cells were stimulated with EGF, fixed and stained with anti-Src and anti-TfR antibodies (as described below). Images were imported into ImageJ and a region of interest was created in individual cells by manually tracing the perinuclear TfR to mark the ERC region. Src fluorescence was quantified using the 'measure' function. All cells (control and KD cells in individual experiments) were fixed, stained and imaged on the same day under identical confocal settings.

Src recruitment to PDGF-induced CDRs (15 CDRs per condition per experiment, three independent experiments in total) was quantified from Src- and actin-fluorescence values that were measured by profile line-scan analysis in Pascal LSM5 Image Examiner. The data were expressed as a ratio of Src fluorescence to actin fluorescence. The total MICAL-L1-containing tubule area was calculated as described previously (Cai et al., 2013).

Immunoblotting

Cells were washed twice in ice-cold PBS and were then scraped off the plate with a rubber policeman into ice-cold RIPA buffer (50 mM Tris-HCl, 150 mM NaCl, 5 mM EDTA, 1% Triton X-100, 0.5% sodium deoxycholate, 0.1% SDS, 1.8 mg/ml iodoacetamide, 1 mM orthovanadate, 2.5 mM sodium pyrophosphate, 1 mM glycerophosphate, 1 µg/ml leupeptin, 5 µg/ml aprotinin, 1 mM PMSF). Lysates were then clarified by centrifugation at 21,130 ***g*** at 4℃. Protein levels were quantified using the BCA assay (BioRad). For immunoblotting, 20–30 µg (HeLa cells) or 10–15 µg (BJ cells) of each protein lysate was separated by 8% SDS-PAGE. Proteins were transferred onto nitrocellulose membranes. Membranes were blocked for 1 h at room temperature in TBST (TBS with 0.1% Tween). The membranes were incubated overnight in primary antibodies diluted in either TBST plus 3% BSA (for phosphorylated proteins) or TBST plus 5% dried milk. Membranes were washed with TBST and then incubated with HRP-conjugated goat anti-mouse-IgG (Jackson Research Laboratories) or donkey anti-rabbit-IgG (GE Healthcare) secondary antibody for 1 h at room temperature.

Cell spreading

At 72 h post-siRNA transfection, BJ cells were detached from plates with 0.05% trypsin-EDTA. Trypsin was inactivated by the addition of complete growth medium. The cells were pelleted and washed twice in serum-free medium and then incubated in suspension at 37℃ for 30 min. Cells were then plated onto 10 µg/ml fibronectin-coated coverslips for 90 min. For immunoblots, cells in suspension were plated onto fibronectin-coated tissue culture dishes and harvested at the timepoints indicated in the text. The cell area was measured using Pascal LSM Image Examiner by manually tracing borders around cells. Focal adhesions were quantified as described below.

Focal adhesion quantification

The number and size of focal adhesions was measured in ImageJ. Images from vinculin-stained samples were imported into ImageJ. Cropped images of single cells were assessed with a common threshold. The total number of focal adhesions per cell was quantified using the 'measure particles' function with the parameters set to measure particles of 1–30 μm^2. The size distribution of focal adhesions was analyzed by categorizing focal adhesion area into three categories: 1–5 μm^2, 6–10 μm^2 and 11–30 μm^2.

Scratch wound assay

At 48 h post-siRNA transfection, BJ cells were trypsinized and plated onto 10 µg/ml fibronectin-coated coverslips at high density in low-serum (2%) medium overnight. A single scratch was made using a P200 pipet tip. Cell debris was washed away with low-serum medium and the cells were then incubated in low-serum medium for the times indicated in the text prior to fixation.

Flow cytometry

At 48 h post-siRNA transfection, control and MICAL-L1-KD cells were trypsinized. Trypsin was inactivated by addition of complete serum. Cells were pelleted and washed twice with serum-free medium. Cells were incubated in suspension in serum-free medium for 1 h at 37℃. Cells were then pelleted at 4℃ and resuspended in ice-cold serum-free medium containing 1 µg/ml EGF–Rhodamine and incubated at 4℃ with gentle rotation. Cells were pelleted, washed three times with cold PBS and fixed with 4% paraformaldehyde. At least 10,000 cells were analyzed for surface-bound EGF–Rhodamine by flow cytometry analysis (BD Biosciences).

Immunofluoresence

Cells were treated as indicated in the text and then fixed in 3.7% paraformaldehyde in PBS (HeLa) or PHEM (60 mM PIPES, 25 mM HEPES, 10 mM EGTA, 2 mM $MgCl_2$, pH 7.0) for 15 min at room temperature. Cells were rinsed three times in PBS and permeabilized in PBS containing 0.1% Triton X-100 for 3 min (HeLa) or 10 min (BJ). Cells were then blocked for 1 h at room temperature in PBS containing 10% normal goat serum, 1% BSA and 0.1 M glycine. The cells were incubated with primary antibody in PBS plus 1% BSA and, where indicated, phalloidin–Alexa-Fluor-488 or phalloidin–Rhodamine (Invitrogen), for 1 h at room temperature, washed three times in PBS and then incubated with the appropriate fluorochrome-conjugated secondary antibodies (Molecular Probes) plus DAPI for 1 h at room temperature. Cells were washed three times in PBS and mounted in Fluoromount G.

Single-plane confocal images were collected by using a Zeiss LSM5 Pascal laser confocal microscope with a Plan-Apochromat 63×/1.4 NA oil objective, except for scratch-wound images which were collected by using a Plan-Neofluor 10×/0.3 NA objective. For quantification, collected images were imported into ImageJ or LSM Pascal Image Examiner as described above. The images presented in figures were imported into Adobe Photoshop CS, where they were re-sized and formatted to 300 dpi resolution with minimal image manipulation (whole-image adjustment of brightness was performed using the 'levels' function).

Statistics

Data from ImageJ was imported into Microsoft Excel. The mean and the standard error of the mean were calculated from data obtained from three independent experiments. Statistical significance was calculated by one-way ANOVA and Tukey test (when comparing more than two samples) using the Vassarstats program (http://www.vassarstats.net).

Acknowledgements

We thank E. Caplan (Omaha, NE) for critical reading of this manuscript, Victoria Smith and the UNMC Cell Analysis Facility for help with flow cytometry (UNMC, Omaha, NE, USA), and Viola Lobert (Oslo University Hospital Montebello, Oslo, Norway) and Radoslav Janostiak (Charles University in Prague Prague, Czech Republic) for helpful discussions.

Competing interests

The authors declare no competing interests.

Author contributions

J.B.R. carried out the majority of the experiments, prepared the figures and wrote the manuscript. D.K. assisted in carrying out a number of the experiments and prepared key reagents required for several figures in the manuscript. N.N. and S.C. jointly directed the study, assisted in figure preparation, manuscript preparation and editing.

Funding

This work was supported by a National Institute of General Medical Sciences grant from the National Institutes of Health [grant number RO1GM087455]; a grant from the Nebraska Department of Health; and a University of Nebraska Medical Centre graduate fellowship (to J.B.R.). Deposited in PMC for release after 12 months.

Supplementary material

Supplementary material available online at
http://jcs.biologists.org/lookup/suppl/doi:10.1242/jcs.133892/-/DC1

References

Arias-Salgado, E. G., Lizano, S., Sarkar, S., Brugge, J. S., Ginsberg, M. H. and Shattil, S. J. (2003). Src kinase activation by direct interaction with the integrin beta cytoplasmic domain. *Proc. Natl. Acad. Sci. USA* **100**, 13298-13302.

Azimifar, S. B., Böttcher, R. T., Zanivan, S., Grashoff, C., Krüger, M., Legate, K. R., Mann, M. and Fässler, R. (2012). Induction of membrane circular dorsal ruffles requires co-signalling of integrin-ILK-complex and EGF receptor. *J. Cell Sci.* **125**, 435-448.

Cai, B., Giridharan, S. S., Zhang, J., Saxena, S., Bahl, K., Schmidt, J. A., Sorgen, P. L., Guo, W., Naslavsky, N. and Caplan, S. (2013). Differential roles of C-terminal Eps15 homology domain proteins as vesiculators and tubulators of recycling endosomes. *J. Biol. Chem.* **288**, 30172-30180.

Caplan, S., Naslavsky, N., Hartnell, L. M., Lodge, R., Polishchuk, R. S., Donaldson, J. G. and Bonifacino, J. S. (2002). A tubular EHD1-containing compartment involved in the recycling of major histocompatibility complex class I molecules to the plasma membrane. *EMBO J.* **21**, 2557-2567.

Chang, J. H., Gill, S., Settleman, J. and Parsons, S. J. (1995). c-Src regulates the simultaneous rearrangement of actin cytoskeleton, p190RhoGAP, and p120RasGAP following epidermal growth factor stimulation. *J. Cell Biol.* **130**, 355-368.

Cooper, J. A., Gould, K. L., Cartwright, C. A. and Hunter, T. (1986). Tyr527 is phosphorylated in pp60c-src: implications for regulation. *Science* **231**, 1431-1434.

Courtneidge, S. A., Levinson, A. D. and Bishop, J. M. (1980). The protein encoded by the transforming gene of avian sarcoma virus (pp60src) and a homologous protein in normal cells (pp60proto-src) are associated with the plasma membrane. *Proc. Natl. Acad. Sci. USA* **77**, 3783-3787.

Deramaudt, T. B., Dujardin, D., Hamadi, A., Noulet, F., Kolli, K., De Mey, J., Takeda, K. and Rondé, P. (2011). FAK phosphorylation at Tyr-925 regulates cross-talk between focal adhesion turnover and cell protrusion. *Mol. Biol. Cell* **22**, 964-975.

Donepudi, M. and Resh, M. D. (2008). c-Src trafficking and co-localization with the EGF receptor promotes EGF ligand-independent EGF receptor activation and signaling. *Cell. Signal.* **20**, 1359-1367.

Ezratty, E. J., Partridge, M. A. and Gundersen, G. G. (2005). Microtubule-induced focal adhesion disassembly is mediated by dynamin and focal adhesion kinase. *Nat. Cell Biol.* **7**, 581-590.

Feder, D. and Bishop, J. M. (1990). Purification and enzymatic characterization of pp60c-src from human platelets. *J. Biol. Chem.* **265**, 8205-8211.

Fichtman, B., Ravid, L., Rapaport, D. and Horowitz, M. (2008). EHDS are serine phosphoproteins: EHD1 phosphorylation is enhanced by serum stimulation. *Cell. Mol. Biol. Lett.* **13**, 632-648.

Fincham, V. J. and Frame, M. C. (1998). The catalytic activity of Src is dispensable for translocation to focal adhesions but controls the turnover of these structures during cell motility. *EMBO J.* **17**, 81-92.

Fincham, V. J., Brunton, V. G. and Frame, M. C. (2000). The SH3 domain directs acto-myosin-dependent targeting of v-Src to focal adhesions via phosphatidylinositol 3-kinase. *Mol. Cell. Biol.* **20**, 6518-6536.
Fra, A. M., Williamson, E., Simons, K. and Parton, R. G. (1994). Detergent-insoluble glycolipid microdomains in lymphocytes in the absence of caveolae. *J. Biol. Chem.* **269**, 30745-30748.
Friedl, P. and Gilmour, D. (2009). Collective cell migration in morphogenesis, regeneration and cancer. *Nat. Rev. Mol. Cell Biol.* **10**, 445-457.
Giridharan, S. S., Cai, B., Vitale, N., Naslavsky, N. and Caplan, S. (2013). Cooperation of MICAL-L1, syndapin2, and phosphatidic acid in tubular recycling endosome biogenesis. *Mol. Biol. Cell* **24**, 1776-1790.
Gu, Z., Noss, E. H., Hsu, V. W. and Brenner, M. B. (2011). Integrins traffic rapidly via circular dorsal ruffles and macropinocytosis during stimulated cell migration. *J. Cell Biol.* **193**, 61-70.
Hoon, J. L., Wong, W. K. and Koh, C. G. (2012). Functions and regulation of circular dorsal ruffles. *Mol. Cell. Biol.* **32**, 4246-4257.
Huveneers, S. and Danen, E. H. (2009). Adhesion signaling – crosstalk between integrins, Src and Rho. *J. Cell Sci.* **122**, 1059-1069.
Jović, M., Naslavsky, N., Rapaport, D., Horowitz, M. and Caplan, S. (2007). EHD1 regulates beta1 integrin endosomal transport: effects on focal adhesions, cell spreading and migration. *J. Cell Sci.* **120**, 802-814.
Kaplan, K. B., Swedlow, J. R., Varmus, H. E. and Morgan, D. O. (1992). Association of p60c-src with endosomal membranes in mammalian fibroblasts. *J. Cell Biol.* **118**, 321-333.
Kaplan, K. B., Bibbins, K. B., Swedlow, J. R., Arnaud, M., Morgan, D. O. and Varmus, H. E. (1994). Association of the amino-terminal half of c-Src with focal adhesions alters their properties and is regulated by phosphorylation of tyrosine 527. *EMBO J.* **13**, 4745-4756.
Kasahara, K., Nakayama, Y., Kihara, A., Matsuda, D., Ikeda, K., Kuga, T., Fukumoto, Y., Igarashi, Y. and Yamaguchi, N. (2007). Rapid trafficking of c-Src, a non-palmitoylated Src-family kinase, between the plasma membrane and late endosomes/lysosomes. *Exp. Cell Res.* **313**, 2651-2666.
Klinghoffer, R. A., Sachsenmaier, C., Cooper, J. A. and Soriano, P. (1999). Src family kinases are required for integrin but not PDGFR signal transduction. *EMBO J.* **18**, 2459-2471.
Koegl, M., Zlatkine, P., Ley, S. C., Courtneidge, S. A. and Magee, A. I. (1994). Palmitoylation of multiple Src-family kinases at a homologous N-terminal motif. *Biochem. J.* **303**, 749-753.
Kypta, R. M., Goldberg, Y., Ulug, E. T. and Courtneidge, S. A. (1990). Association between the PDGF receptor and members of the src family of tyrosine kinases. *Cell* **62**, 481-492.
Lobert, V. H. and Stenmark, H. (2012). The ESCRT machinery mediates polarization of fibroblasts through regulation of myosin light chain. *J. Cell Sci.* **125**, 29-36.
Luttrell, D. K., Lee, A., Lansing, T. J., Crosby, R. M., Jung, K. D., Willard, D., Luther, M., Rodriguez, M., Berman, J. and Gilmer, T. M. (1994). Involvement of pp60c-src with two major signaling pathways in human breast cancer. *Proc. Natl. Acad. Sci. USA* **91**, 83-87.
Magdalena, J., Millard, T. H. and Machesky, L. M. (2003). Microtubule involvement in NIH 3T3 Golgi and MTOC polarity establishment. *J. Cell Sci.* **116**, 743-756.
Mettlen, M., Platek, A., Van Der Smissen, P., Carpentier, S., Amyere, M., Lanzetti, L., de Diesbach, P., Tyteca, D. and Courtoy, P. J. (2006). Src triggers circular ruffling and macropinocytosis at the apical surface of polarized MDCK cells. *Traffic* **7**, 589-603.
Mori, S., Rönnstrand, L., Yokote, K., Engström, A., Courtneidge, S. A., Claesson-Welsh, L. and Heldin, C. H. (1993). Identification of two juxtamembrane autophosphorylation sites in the PDGF beta-receptor; involvement in the interaction with Src family tyrosine kinases. *EMBO J.* **12**, 2257-2264.
Nada, S., Okada, M., MacAuley, A., Cooper, J. A. and Nakagawa, H. (1991). Cloning of a complementary DNA for a protein-tyrosine kinase that specifically phosphorylates a negative regulatory site of p60c-src. *Nature* **351**, 69-72.
Payne, G., Shoelson, S. E., Gish, G. D., Pawson, T. and Walsh, C. T. (1993). Kinetics of p56lck and p60src Src homology 2 domain binding to tyrosine-phosphorylated peptides determined by a competition assay or surface plasmon resonance. *Proc. Natl. Acad. Sci. USA* **90**, 4902-4906.
Rahajeng, J., Giridharan, S. S., Naslavsky, N. and Caplan, S. (2010). Collapsin response mediator protein-2 (Crmp2) regulates trafficking by linking endocytic regulatory proteins to dynein motors. *J. Biol. Chem.* **285**, 31918-31922.
Ren, Y., Meng, S., Mei, L., Zhao, Z. J., Jove, R. and Wu, J. (2004). Roles of Gab1 and SHP2 in paxillin tyrosine dephosphorylation and Src activation in response to epidermal growth factor. *J. Biol. Chem.* **279**, 8497-8505.
Reuter, C., Findik, D. and Presek, P. (1990). Characterization of purified pp60c-src protein tyrosine kinase from human platelets. *Eur. J. Biochem.* **190**, 343-350.
Rohrschneider, L. R. (1979). Immunofluorescence on avian sarcoma virus-transformed cells: localization of the src gene product. *Cell* **16**, 11-24.
Sandilands, E. and Frame, M. C. (2008). Endosomal trafficking of Src tyrosine kinase. *Trends Cell Biol.* **18**, 322-329.
Sandilands, E., Cans, C., Fincham, V. J., Brunton, V. G., Mellor, H., Prendergast, G. C., Norman, J. C., Superti-Furga, G. and Frame, M. C. (2004). RhoB and actin polymerization coordinate Src activation with endosome-mediated delivery to the membrane. *Dev. Cell* **7**, 855-869.
Schnatwinkel, C., Christoforidis, S., Lindsay, M. R., Uttenweiler-Joseph, S., Wilm, M., Parton, R. G. and Zerial, M. (2004). The Rab5 effector Rabankyrin-5 regulates and coordinates different endocytic mechanisms. *PLoS Biol.* **2**, E261.
Sharma, M., Giridharan, S. S., Rahajeng, J., Naslavsky, N. and Caplan, S. (2009). MICAL-L1 links EHD1 to tubular recycling endosomes and regulates receptor recycling. *Mol. Biol. Cell* **20**, 5181-5194.
Smart, J. E., Oppermann, H., Czernilofsky, A. P., Purchio, A. F., Erikson, R. L. and Bishop, J. M. (1981). Characterization of sites for tyrosine phosphorylation in the transforming protein of Rous sarcoma virus (pp60v-src) and its normal cellular homologue (pp60c-src). *Proc. Natl. Acad. Sci. USA* **78**, 6013-6017.
Tanji, M., Ishizaki, T., Ebrahimi, S., Tsuboguchi, Y., Sukezane, T., Akagi, T., Frame, M. C., Hashimoto, N., Miyamoto, S. and Narumiya, S. (2010). mDia1 targets v-Src to the cell periphery and facilitates cell transformation, tumorigenesis, and invasion. *Mol. Cell. Biol.* **30**, 4604-4615.
Timpson, P., Jones, G. E., Frame, M. C. and Brunton, V. G. (2001). Coordination of cell polarization and migration by the Rho family GTPases requires Src tyrosine kinase activity. *Curr. Biol.* **11**, 1836-1846.
Tu, C., Ortega-Cava, C. F., Winograd, P., Stanton, M. J., Reddi, A. L., Dodge, I., Arya, R., Dimri, M., Clubb, R. J., Naramura, M. et al. (2010). Endosomal-sorting complexes required for transport (ESCRT) pathway-dependent endosomal traffic regulates the localization of active Src at focal adhesions. *Proc. Natl. Acad. Sci. USA* **107**, 16107-16112.
Veracini, L., Franco, M., Boureux, A., Simon, V., Roche, S. and Benistant, C. (2006). Two distinct pools of Src family tyrosine kinases regulate PDGF-induced DNA synthesis and actin dorsal ruffles. *J. Cell Sci.* **119**, 2921-2934.
Ware, M. F., Tice, D. A., Parsons, S. J. and Lauffenburger, D. A. (1997). Overexpression of cellular Src in fibroblasts enhances endocytic internalization of epidermal growth factor receptor. *J. Biol. Chem.* **272**, 30185-30190.
Webb, D. J., Donais, K., Whitmore, L. A., Thomas, S. M., Turner, C. E., Parsons, J. T. and Horwitz, A. F. (2004). FAK-Src signalling through paxillin, ERK and MLCK regulates adhesion disassembly. *Nat. Cell Biol.* **6**, 154-161.
Welham, M. J. and Wyke, J. A. (1988). A single point mutation has pleiotropic effects on pp60v-src function. *J. Virol.* **62**, 1898-1906.
Wheeler, D. L., Iida, M. and Dunn, E. F. (2009). The role of Src in solid tumors. *Oncologist* **14**, 667-678.
Wilde, A., Beattie, E. C., Lem, L., Riethof, D. A., Liu, S. H., Mobley, W. C., Soriano, P. and Brodsky, F. M. (1999). EGF receptor signaling stimulates SRC kinase phosphorylation of clathrin, influencing clathrin redistribution and EGF uptake. *Cell* **96**, 677-687.
Wozniak, M. A., Modzelewska, K., Kwong, L. and Keely, P. J. (2004). Focal adhesion regulation of cell behavior. *Biochim. Biophys. Acta* **1692**, 103-119.
Xu, W., Doshi, A., Lei, M., Eck, M. J. and Harrison, S. C. (1999). Crystal structures of c-Src reveal features of its autoinhibitory mechanism. *Mol. Cell* **3**, 629-638.